2010

Lithium- and Oxygen- Isotope Profiles of a Mid-Atlantic Ridge Oceanic Core Complex: The Atlantis Massif, 30°N

Ellen J. Crapster-Pregont
Colby College

LITHIUM- AND OXYGEN-ISOTOPE PROFILES OF A MID-ATLANTIC RIDGE OCEANIC CORE COMPLEX: THE ATLANTIS MASSIF, 30°N

Except where reference is made to the work of others, the work described in this thesis is my own or was conducted in collaboration with my advisory committee

Ellen J. Crapster-Pregont ‘10

Certificate of Approval:

Dr. Valerie S. Reynolds
Clare Boothe Luce Assistant Professor
Department of Geology

Dr. Robert A. Gastaldo, Chair
Whipple Coddington Professor
Department of Geology

Dr. Walter A. Sullivan
Assistant Professor
Department of Geology

Dr. D. Whitney King, Chair
Miselis Professor
Department of Chemistry

LITHIUM- AND OXYGEN-ISOTOPE PROFILES OF A MID-ATLANTIC RIDGE OCEANIC CORE COMPLEX: THE ATLANTIS MASSIF, 30°N

Ellen J. Crapster-Pregont ‘10

A Thesis

Submitted to the Faculty of the Geology Department of
Colby College in Fulfillment of the Requirements for
Honors in Geology

Waterville, Maine

May 7, 2010

ABSTRACT

Oxygen (O) and lithium (Li) are fluid-mobile elements used as geochemical tracers of a crustal component in the mantle. The isotopes of each element fractionate according to the degree and temperature of hydrothermal alteration. Previous studies demonstrate that Li and O isotopic trends are coupled within the upper crust near mid-ocean ridges but are decoupled in subduction-related volcanism. To better understand the average crustal signature of these systems, it is necessary to characterize these systems in the presently poorly understood lower oceanic crust. This study uses lower crustal samples from IODP Expedition 305 Hole U1309D exhumed at the Atlantis Massif, 30°N.

Oxygen isotope values range from 0.985 to 5.045 ‰ whereas lithium isotope values range from -2.7 to 2.6 ‰. These values are coupled with depth for most samples and are significantly lower than the unaltered MORB values of 5.5 ‰ for oxygen and 4.0 ‰ for lithium. This indicates that high-temperature alteration affected both lithium and oxygen within the core complex. Heavy lithium isotope outlier values of, 6.1 ‰ and 7.1 ‰, are interpreted to have been affected by fluids with evolved compositions. Lithium concentration data range from 1.32 to 12.37 ppm and exhibit no systematic trend or correlation with lithium isotopes, indicating that lithium concentration is independent of hydrothermal alteration. When compared to other deep-sea drill core samples of the lower crust, trends in oxygen isotopes with depth in Expedition 305 drill core vary significantly. The heterogeneity in the geochemical tracer signatures of the lower crust could significantly affect interpretations of crustal recycling into the mantle or continental crust at subduction zones. To obtain a better understanding of this heterogeneity and obtain a better lower-crustal average for geochemical tracers, it is imperative to study the isotopic signatures in lower oceanic crust at spreading centers in various ocean basins.

ACKNOWLEDGEMENTS

The tasks of developing a laboratory and method able to produce reliable data were daunting, and I owe my success to many individuals who lent me their assistance along the way. The breadth of classwork available from the departments of Geology and Chemistry at Colby College has provided a means for me to gain general knowledge regarding the topics, techniques, and funding necessary for conducting my honors research. From the Chemistry Department, I would like to acknowledge Dr. Whitney King and Dr. Thomas Shattuck for answering my questions and assisting in operation of the ICP-OES. From the Geology Department, I would like to thank Dr. Walter Sullivan and Dr. Robert Gastaldo for generously reading and commenting on my thesis. Finally, I thank Professor Emeritus Dr. Don Allen for his undying curiosity and SEM knowledge.

For determining the lithium isotopes, thanks to Dr. William McDonough and PhD candidate Lin Qiu of the University of Maryland. A special thanks to Dr. Doug Rumble of the Carnegie Institution of Washington for running the oxygen isotopes and expressing continued interest in the project.

I must thank my family and friends, who have supported me in all of my endeavors. My parents have always encouraged me to pursue my interests, no matter how strange; my sisters, who have entertained me all these years, have also kept me sane. Thank you!

Lastly, I would like to extend sincere gratitude to my advisor, Dr. Valerie Reynolds, for proposing this project and learning alongside me. Without her guidance and inspiration the project would not have been possible. In always demanding excellence, Valerie guided me to the field of research in which I hope to build my career. Dr. Reynolds, thank you for your time, expertise, and patience.

TABLE OF CONTENTS

LIST OF FIGURES

LIST OF TABLES

LIST OF APPENDICES

INTRODUCTION

Plate tectonics is the driving force that redistributes elements between the Earth's surface and its interior. Distinct chemical signatures develop as young, oceanic crust reacts with seawater at mid-ocean ridges. Such reactions tend to convert anhydrous minerals, such as pyroxene and plagioclase, to an altered hydrous mineral assemblage dominated by chlorite, amphibole, and serpentine (Gillis et al., 2001; Kelley et al., 2005; Winter, 2001). As these reactions proceed, elemental and isotopic exchange between the oceanic crust and seawater results in altered crust that is chemically distinct from its mantle source. As altered, hydrous oceanic crust enters a subduction zone, increased temperatures at depth initiate dehydration reactions that transfer water and fluid-mobile elements, such as lithium, from the subducting slab to the overlying mantle wedge. Elements that are not fluid mobile, however, remain in the slab and are carried deeper into the Earth's interior. The distinct chemistry of altered oceanic crust can influence the composition of the mantle source regions that melt to produce lava, thereby providing a means to identify a component of recycled crust in the mantle.

Lithium (Li) and oxygen (O) are two stable, fluid-mobile elements that have been utilized independently to track a component of recycled crust in the mantle source regions of lavas erupted in island-arc and ocean-island environments (Chan and Frey, 2003; Elliot et al., 2004; Kobayashi et al., 2004; Ryan and Kyle, 2004; Tomascak et al., 2000; Williams et al., 2009). The ability for these two elements to record recycled crust in the mantle relies on their isotopic fractionation behavior during hydrothermal alteration at mid-ocean ridges. The extent to which a particular section of oceanic crust is hydrothermally altered depends on the

temperature and depth to which fluids penetrate as well as the volume of water moving through the rock. The depth and degree of alteration depends on the development of faults and fractures and, by association, spreading rate. Extension at fast-spreading centers (full spreading rate 80-120 mm/year) is driven primarily by magmatic eruptions whereas slow-spreading centers (10-55 mm/year) experience periods of magmatic (~90%) and amagmatic (~10%) extension (Escartin et al., 1999). During amagmatic intervals, extension is accommodated by large-scale normal faults that propagate deep into the crust and act as pathways for seawater circulation (Escartin et al., 1999; Gao et al., 2006).

The isotopes of oxygen and, to a lesser extent, lithium have been studied in the extrusive (basaltic), upper oceanic crust (up to 1500 meters below the seafloor (mbsf)) via deep-sea drilling and exhumation of ophiolites. The intrusive (gabbroic), lower oceanic crust (1500 to 7000 mbsf) remains somewhat enigmatic due to the rarity of lower-crust surface exposures in ophiolite sequences and the complications that are inherent in deep-sea drilling projects (Wilson et al., 2006). Similar fractionation behavior of lithium- and oxygen-isotopes indicate these isotopic systems are coupled in the upper crust at spreading centers (Chan et al., 2002). However, the isotopic signatures of the two systems are decoupled in mantle-derived lavas from island arcs and ocean islands (Chan and Frey, 2003). It is unclear whether this discrepancy occurs due to dehydration reactions during subduction or a lack of coupling in the entire oceanic crust.

Slow-spreading centers often are associated with low-angle normal faults, or detachment faults, that expose the lower crust at the surface as oceanic core complexes (OCC). The goal of this study is to analyze the whole-rock Li and O isotopic compositions of lower-crustal rocks retrieved from Integrated Oceanic Drilling Program (IODP)

Expedition 305 Hole U1309D that samples an OCC along the Mid-Atlantic Ridge. Lithium- and oxygen-isotope signatures are examined with depth in the drill core to determine whether there is a systematic variation in isotopic composition with depth in lower oceanic crust, similar to that observed in the upper crust. Characterizing Li and O isotopes within the lower oceanic crust will contribute toward a greater understanding of lower crustal chemistry, and aid in determining the cause for Li and O isotopes observed in lavas from subduction zones and ocean islands. Results are compared with data derived from other exposures of the lower oceanic crust at slow- and fast-spreading centers.

Structure of the Oceanic Crust and Oceanic Core Complexes

Present knowledge of the physical structure of the oceanic crust is obtained from seismic studies and ophiolite sequences. Ophiolites allow the structure, petrography, and morphology of the oceanic crust and uppermost mantle to be studied. The rocks found in a typical oceanic crustal sequence can be grouped into four layers (Figure 1) (Winter, 2001). Layer 1, the uppermost, incorporates pelagic, deep-sea sediments that overlie the basement rocks. Layer 2 contains extrusive pillow basalts and associated volcanics, as well as basaltic feeder dikes or sheeted dike complexes. The upper crust is defined as Layers 1 and 2. Layer 3 comprises the lower crust and consists of massive gabbro overlying layered mafic pyroxene and olivine cumulates. The deepest layer, Layer 4, is composed of ultramafic rocks, such as peridotite, harzburgite, and dunite, and is considered to be the uppermost portion of the mantle that partially melted to form the crust. The petrologic Mohorovičić Discontinuity (Moho) lies between Layers 3 and 4 and represents an increase in seismic velocity. The total

thickness of the oceanic crust, Layers 1 through 4, varies inversely with spreading rate and position along the ridge axis (Escartin et al., 1999; Wilson et al., 2006).

The average depth to lower oceanic crust (approximately 2 km) typically exceeds the present capability of deep-sea drilling projects. However, the lower oceanic crust is exhumed naturally as OCCs, which form during amagmatic extension of slow-spreading ridges, on the inside corner of intersections between transform faults and spreading segments (Escartin et al., 1999; Tremblay et al., 2009). OCC formation is initiated by steeply dipping normal faults that propagate until reaching a zone of ductile shear in the uppermost section of the mantle (Figure 2A). Tectonic unloading causes the footwall to rebound, which rotates the fault to a subhorizontal position resulting in a low-angle fault (Figure 2B to 2C). As the fault continues to propagate in the ductile zone, plastic material swells forming a rounded mound or massif. Related stress causes secondary normal faulting (Figure 2C). A new normal fault is then initiated when the first detachment becomes inactive (Figure 2D). This form of amagmatic extension ceases when volcanism resumes and the OCC migrates away from the spreading ridge (Tremblay et al., 2009).

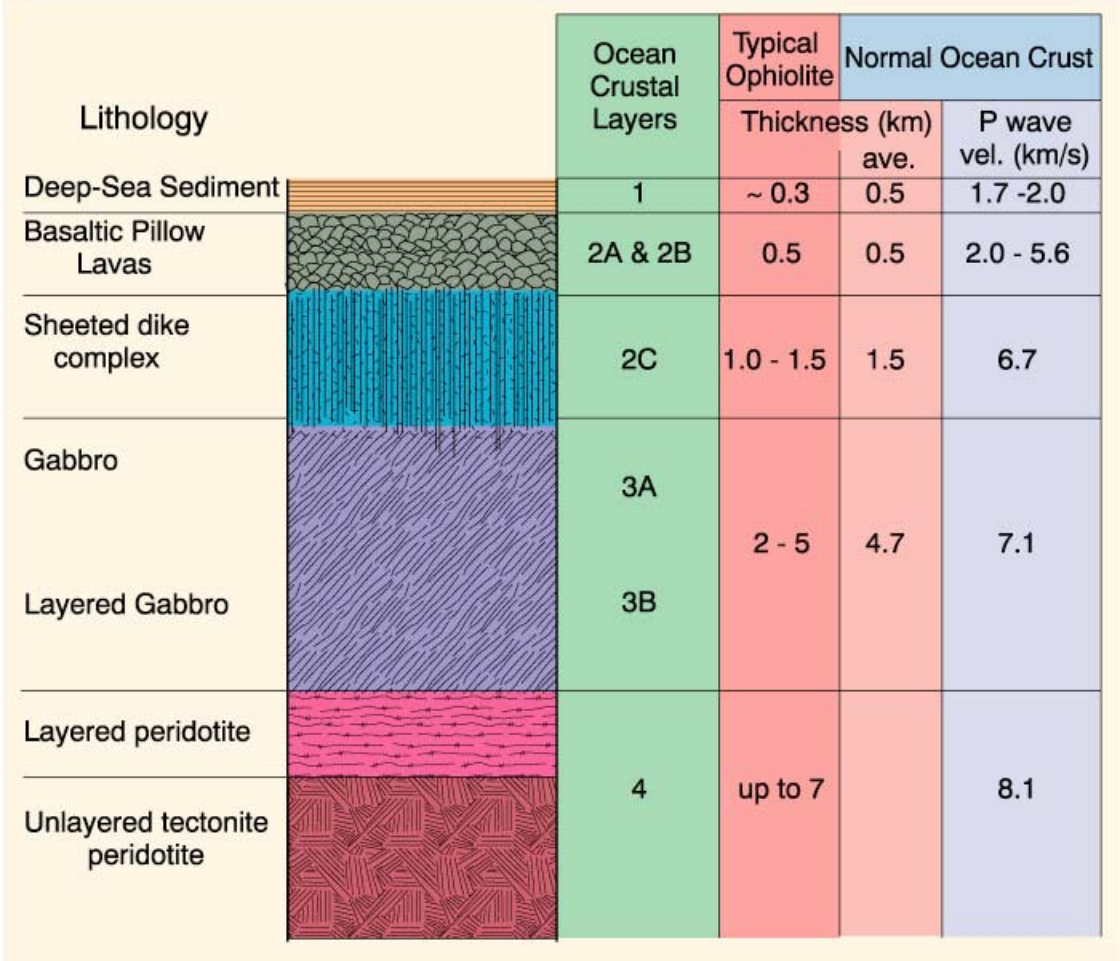

Figure 1: Simplified schematic of the structure of the oceanic crust. Layers are labeled with expected rock type, average depth, and P-wave velocity. Image unmodified from Winter (2001).

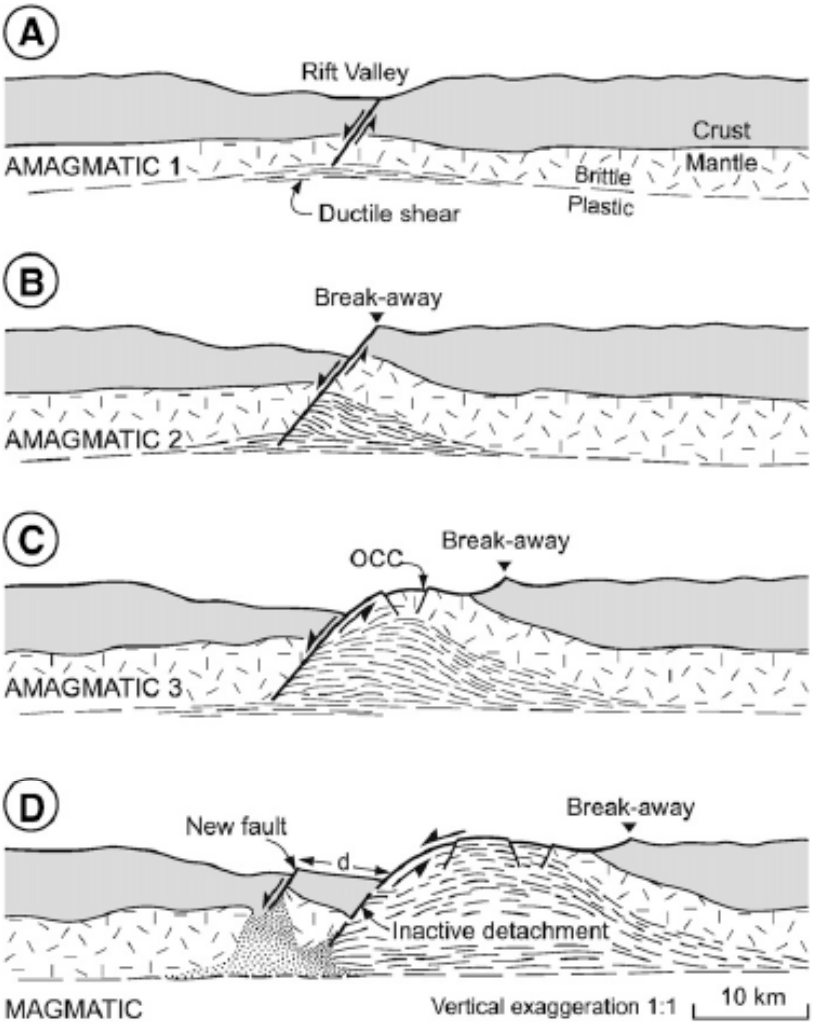

Figure 2: Schematic illustrating the formation of an oceanic core complex (OCC) via the rolling hinge model. Unloading of upper volcanic material causes lower crustal material to isostatically rebound and become exposed at the water-rock interface. Image unmodified from Tremblay et al. (2009).

Spreading Rate and Hydrothermal Alteration

Whether an element or isotope fractionates into seawater or rock depends on its partitioning behavior, the volume and temperature of fluids circulating through the oceanic crust, and the depth of circulation (Eiler, 2001; Tang et al., 2007). The extent to which seawater penetrates the oceanic crust depends on the frequency and depth of fractures and faults present at a mid-ocean ridge (MOR). Fluid temperature varies primarily with proximity to the magma source, although the latent heat of crystallization of alteration minerals may contribute to this parameter.

Fast-spreading centers (80-120 mm/year) are characterized by intermittent periods of intense volcanism and vent formation associated with high rates of crustal formation (Shanks, 2001). Dike intrusions act as the heat source driving circulation of fluids within the crust at these sites (Wilcock and Delaney, 1996). However, the high rate of crystallization clogs the vents and prevents prolonged periods of fluid mobility within the rock body before another eruption may occur (Wilcock and Delaney, 1996). The high rates of crustal production also limit the depth of brittle deformation and, therefore, fracture penetration to the upper 2–3 km (Bach and Humphris, 1999). Hydrothermal alteration at fast-spreading ridges is isolated in the upper portions of the crust for the limited time the fractures remain open.

Slow-spreading centers, on the other hand, (10-55 mm/year) are extensional structures producing fractures that penetrate deeper into the crust because brittle deformation occurs to depths of greater than 3 km (Bach and Humphris, 1999; Shanks, 2001; Wilcock and Delaney, 1996). A combination of abundant pathways, copious exposed submarine rock surfaces, and a slow circulation rate increase the flux of fluids at slow-spreading centers

relative to fast-spreading centers (Bach and Humphris, 1999). Close proximity to the magma source prevents the fractures from closing before new ones replace them, providing for the seemingly continuous and extensive amounts of hydrothermal activity observed. The flux of fluids through pathways at slow-spreading centers occurs over an extended period of time to great depth, affecting the duration of water-rock exchanges within the crust (Shanks, 2001).

Oxygen and Lithium in the Oceanic Crust

The Crustal Signature of Oxygen and Lithium Isotopes

For over 30 years, oxygen isotopes have been used to identify recycled crust in the mantle (Eiler, 2001). A unique oxygen isotopic signature in oceanic crust develops during hydrothermal alteration at mid-ocean ridges, but the value depends on the temperature and extent of alteration. During high-temperature (500–900°C) alteration, ^{18}O is leached preferentially from the rock by fluids (i.e., seawater). Conversely, ^{18}O is preferentially extracted from the fluid and retained in alteration minerals during low-temperature (<350°C) alteration. The result is either a positive or negative deviation from the well-characterized upper mantle value for mid-ocean ridge basalt (MORB) compared to standard mean ocean water (SMOW) (Equation 1) ($\delta^{18}O = 5.5 \pm 0.2$ ‰) (Eiler, 2001). The $\delta^{18}O$ of the upper oceanic crust ranges from 7–15 ‰, whereas the $\delta^{18}O$ of the lower oceanic crust is 0–6 ‰ (Eiler, 2001).

$$\delta^{18}O = \left(\frac{\left(\frac{^{18}O}{^{16}O}\right)_{sample} - \left(\frac{^{18}O}{^{16}O}\right)_{SMOW}}{\left(\frac{^{18}O}{^{16}O}\right)_{SMOW}} \right) \times 1000 \quad (1)$$

In the last 20 years, analytical techniques have advanced to a point where light-element concentrations can be determined precisely. Fresh, unaltered MORB has a value for δ^7Li (Equation 2) that ranges from 3–5 ‰ compared to a lithium carbonate standard (L-SVEC) (Tang et al., 2007). Similar to oxygen, lithium isotopes in marine settings fractionate between seawater and oceanic crust during hydrothermal alteration. During high-temperature (500–900°C) alteration, ^{7}Li is leached from the rock, whereas low-temperature (<350°C) hydrothermal alteration results in ^{7}Li being preferentially incorporated into alteration minerals (Tang et al., 2007). Differentiation between high- and low-temperature δ^7Li signatures is not well documented in either the upper or lower oceanic crust but appears, at least in the upper crust, to mimic trends in oxygen.

$$\delta^{7}Li = \left(\frac{\left(\frac{^{7}Li}{^{6}Li}\right)_{sample} - \left(\frac{^{7}Li}{^{6}Li}\right)_{L-SVEC}}{\left(\frac{^{7}Li}{^{6}Li}\right)_{L-SVEC}} \right) \times 1000 \quad (2)$$

Previous Studies of Lithium and Oxygen Isotopes in the Oceanic Crust

Analyses of ophiolite sequences and samples collected by deep-sea drilling expeditions permit characterization of the structure, alteration, and chemistry of the oceanic

crust. The elemental signatures of the upper oceanic crust are well documented while those of the lower oceanic crust are not due to sample inaccessibility (Wilson et al., 2006).

Fast-spreading centers

Deep Sea Drilling Program (DSDP)/ Ocean Drilling Program (ODP) Hole 504B, on the Costa Rica Rift (32.5 mm/year) drilled to a depth of 2111 mbsf into 5.9 Ma crust (Figure 3) (Chan et al., 2002). Chan et al. (2002) compared δ^7Li with δ^{18}O as determined by Alt et al. (1986), and observed a correlation between the deviations from unaltered MORB with depth in the upper oceanic crust (Figure 4). The upper section of the core, which includes pillow and massive basalt flows, exhibits a heavier δ^7Li value than fresh MORB, indicating the occurrence of reaction products formed by low-temperature alteration with seawater. The upper region of the core is enriched in ^{18}O, and the sheeted dike complex is characterized by alternating heavy and light δ^{18}O values (Alt et al., 1986). The δ^7Li value is lighter in the transition zone between crustal Layers 2 and 3, and variable in the sheeted dike complex due to high-temperature reactions. Overall, total Li concentrations decrease with depth (Figure 5) (Chan et al., 2002). Although the isotope ratios vary as a function of rock type within the complex, these elemental data correlate with crustal depth and are similar to results reported from ophiolite sequences (Figure 5) (Chan et al., 2002). However, it is not known whether this correlation extends into the gabbroic layers of the lower oceanic crust.

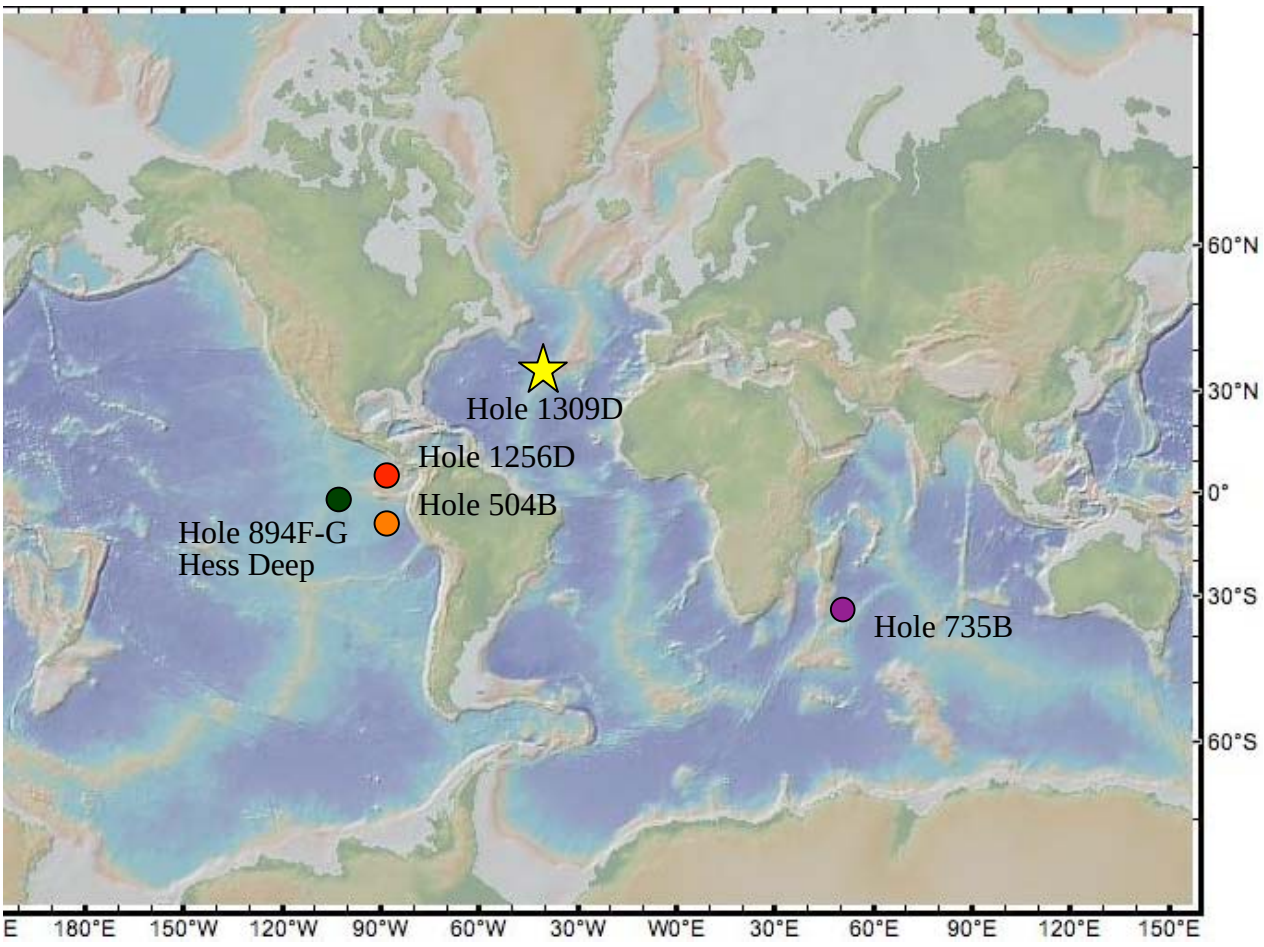

Figure 3: World map depicting major tectonic plates and divergent boundaries with drill cores discussed in the text. Image modified from GeoMapApp.

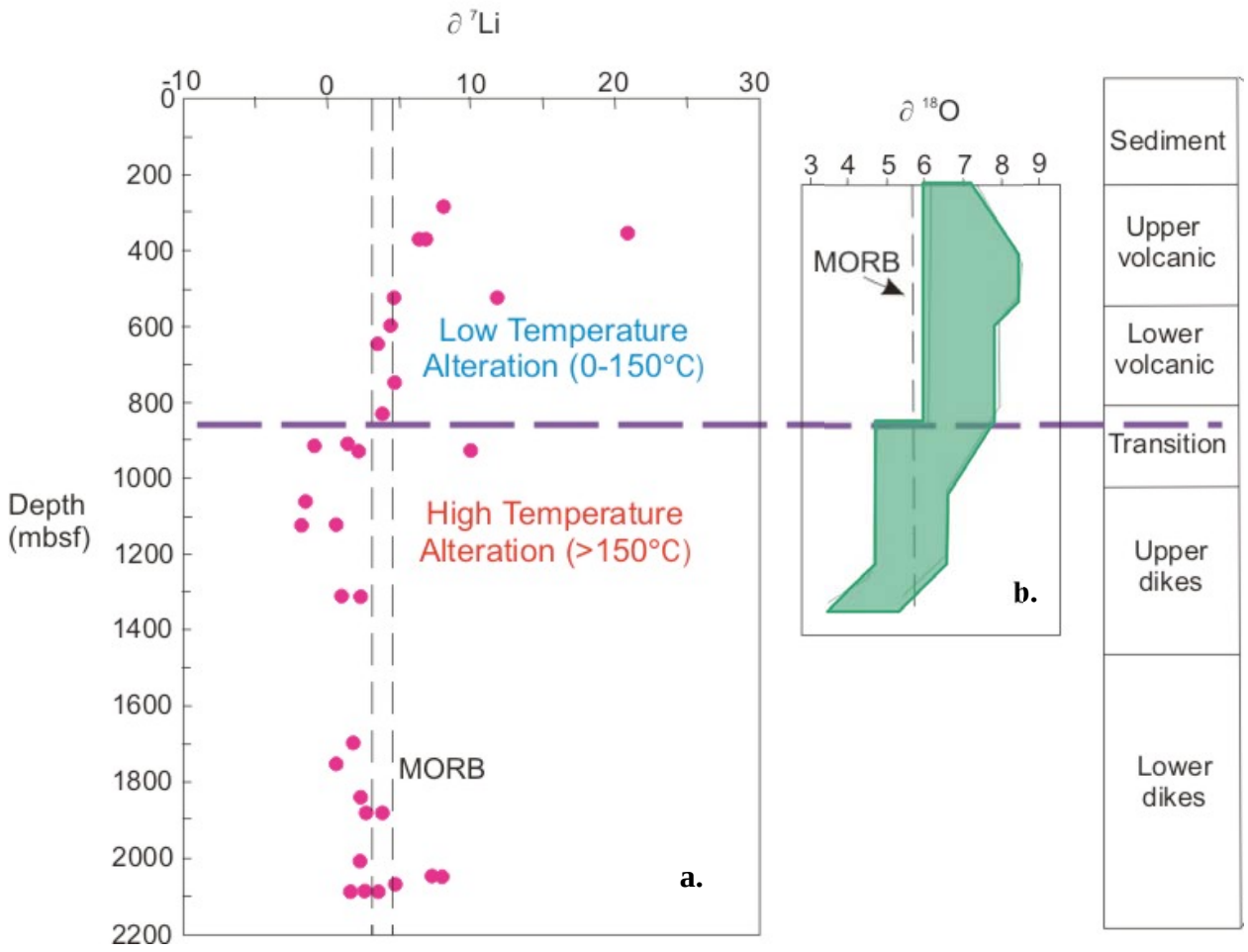

Figure 4: (a) δ^{7}Li and (b) δ^{18}O versus depth in the Hole 504B drill core, located along the Costa Rica Rift. Associated crustal lithology is shown for comparison. Individual δ^{7}Li analyses are shown in pink whereas a range of values is presented for δ^{18}O. δ^{18}O and δ^{7}Li demonstrate similar trends (i.e., are coupled) with depth in the drill core. The upper portion of the drill core experienced low-temperature alteration resulting in heavy δ^{18}O and δ^{7}Li signatures. Conversely, the lower portion records high-temperature alteration resulting in light δ^{18}O and δ^{7}Li signatures. At approximately 1800 mbsf, the oxygen isotopes exhibit limited deviations from unaltered MORB values, indicating limited hydrothermal alteration below this depth. Image compiled and modified from δ^{7}Li and δ^{18}O plots from Chan et al. (2002) and Alt et al. (1986), respectively.

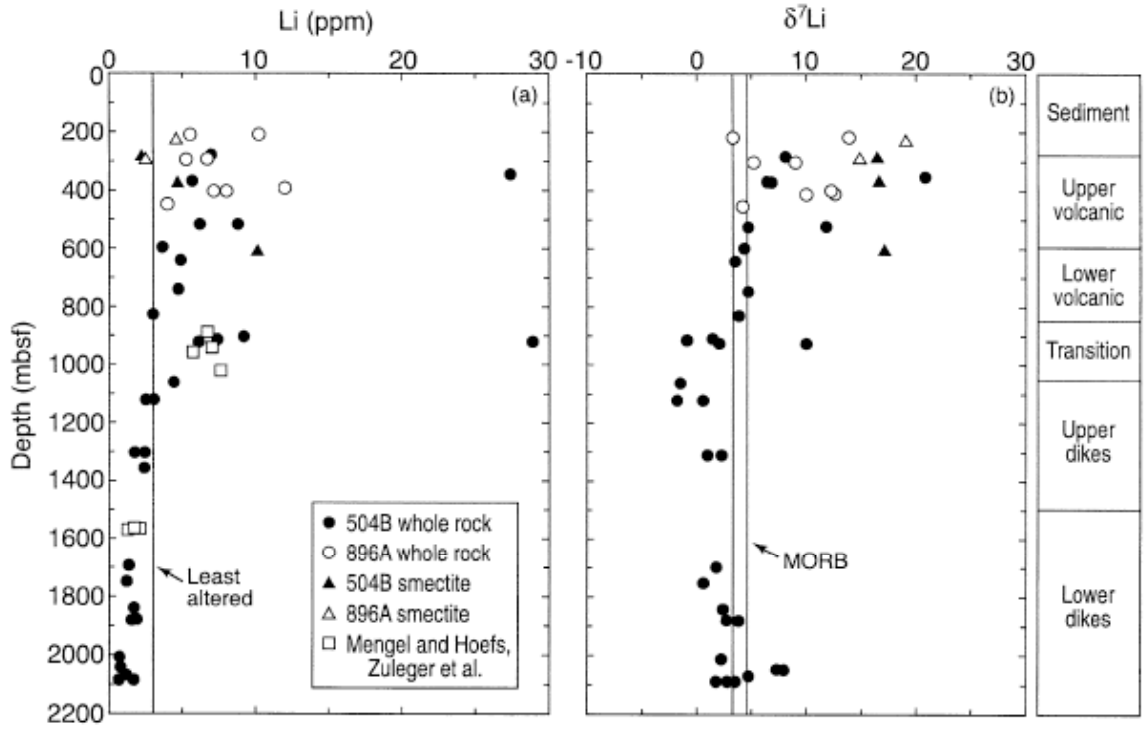

Figure 5: (a) Lithium concentrations (ppm) and (b) δ^7Li with depth in Hole 504B (solid black circles). With depth and increasing temperature of alteration in the drill core, δ^7Li becomes lighter and Li concentrations decrease compared to unaltered MORB. Image unmodified from Chan et al. (2002).

Several sites (Hole 894F-G), around the Hess Deep Rift Valley on the Eastern Pacific Rise (EPR), 2°N 101°W (age 1–2 Ma), allowed for sampling of a fast-spreading center down to the Layer 3 gabbros due to complex tectonic exhumation (Figure 3). These samples exhibit bulk $\delta^{18}O$ that range from 2.2–6.5 ‰, and are generally lighter than unaltered MORB values. The isotopically lightest value occurs at ~105 mbsf and two isotopically heavy samples occur at ~30 mbsf and ~140 mbsf (Figure 6) (Lecuyer and Reynard, 1996).

The only drill core to sample an *in situ* oceanic crustal sequence down to Layer 3 was ODP Expeditions 209/312 Hole 1256D along a superfast-spreading region (220 mm/year) of the EPR (Figure 3) (Wilson et al., 2006). Thinner crust at the superfast-spreading center enabled sampling of a gabbroic layer at 1407 mbsf (total core depth 1507 mbsf). Although bulk-rock major- and trace-element geochemistry was determined for the drill core, lithium- and oxygen-isotope values have not been published (Figure 7) (Gao et al., 2009).

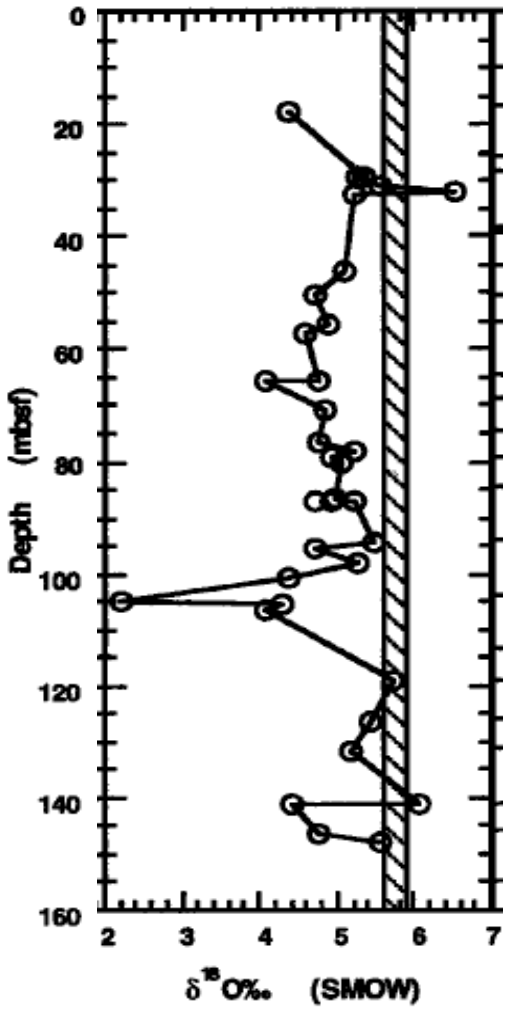

Figure 6: $\delta^{18}O$ with depth in Hole 894F and 894G in the Hess Deep. The hashed region represents the unaltered MORB $\delta^{18}O$ range of ~5.5 to 6 ‰. Image modified from Lecuyer and Reynard (1996).

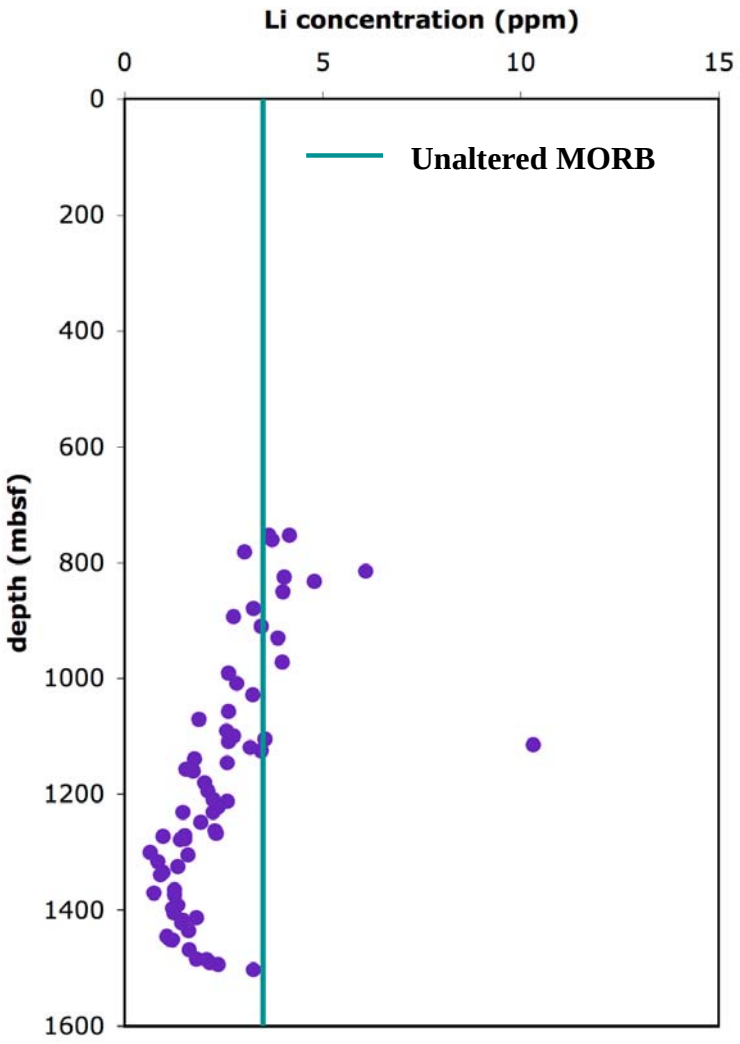

Figure 7: Lithium concentrations (ppm) with depth in Hole 1256D. Data were obtained from shipboard ICP-AES analyses. Lithium values cluster near the unaltered MORB value of ~3.5 ppm. Lithium concentration decreases slightly with depth (800 to 1400 mbsf) then increases below 1400 mbsf. Plot created from data in Gao et al. (2009).

Slow-spreading centers

Hole 735B is located on the southwest (SW) Indian Ridge at an asymmetric slow-spreading center (Figure 3). The drill core penetrated fault-exposed gabbro associated with an OCC (Gao et al., 2006). Alteration is limited to the upper portions of the gabbro layer and the average $\delta^{18}O$ is reported to be 5.5 ‰ (Figure 8) (Gao et al., 2006). Serpentinized peridotites exhibit a range of concentrated fluid-mobile elements, such as Li, compared to unaltered peridotites (Morishita et al., 2009). This indicates that hydrothermal activity, before and after OCC exhumation, influenced the elemental and isotopic composition of the crust. Although Morishita et al. (2009) mention Li as a component of the geochemical suite analyzed, there is no extensive review of Li in the current body of literature for comparison with those for oxygen.

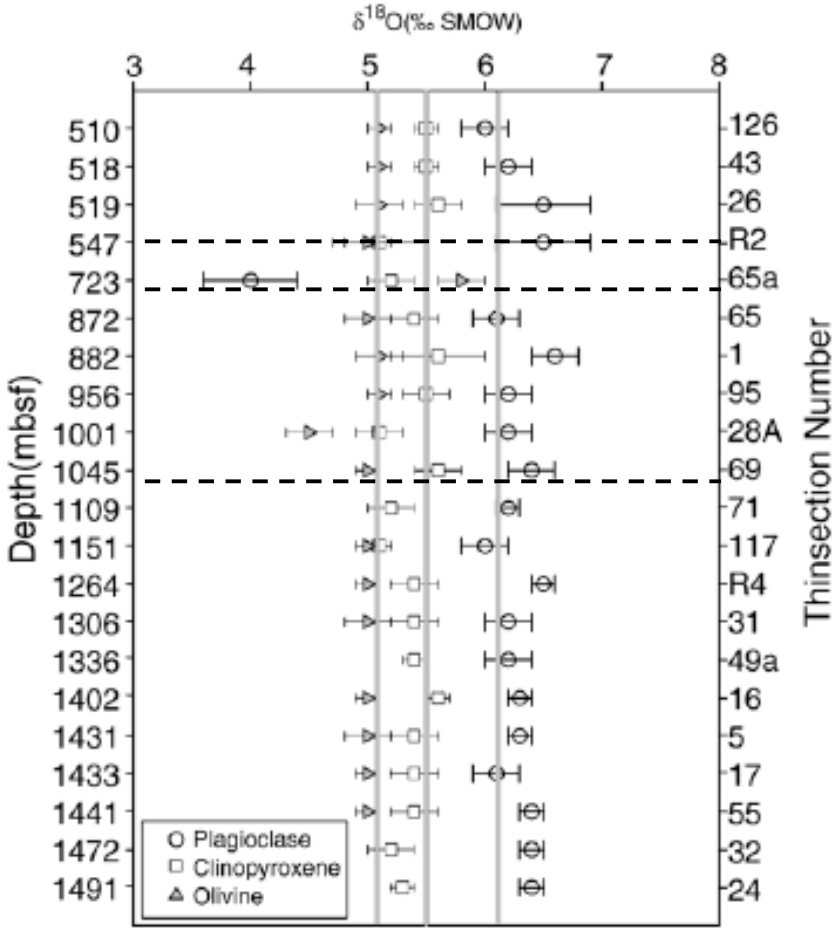

Figure 8: $\delta^{18}O$ for mineral separates with depth for Hole 735B on the SW Indian Ridge. Dashed lines represent fault zones. Solid lines represent $\delta^{18}O$ values for minerals in unaltered MORB. Image modified from Gao et al. (2006).

Study Site: The Atlantis Massif

The core sampled for this study is from the Mid-Atlantic Ridge (MAR) IODP Expedition 305 Hole U1309D, located at the Atlantis Massif that formed 1.5–2 Ma followed by a period of alteration and tectonic activity. The Atlantis Massif is an OCC formed by detachment faulting at the intersection of the Atlantis Transform Fault and the MAR at approximately 30°N (Figures 3 and 9) (Boschi et al., 2006). This section of the MAR has been classified as a slow- to intermediate-spreading center with a full spreading rate of 55 mm/year (Godard et al., 2009). Hole U1309D was drilled into the footwall of the detachment, 30° N, to a depth of 1400 mbsf during two expeditions. Expedition 304 sampled down to 401.3 mbsf and Expedition 305 sampled from 401.3 to 1415.5 mbsf (Ildefonse et al., 2006).

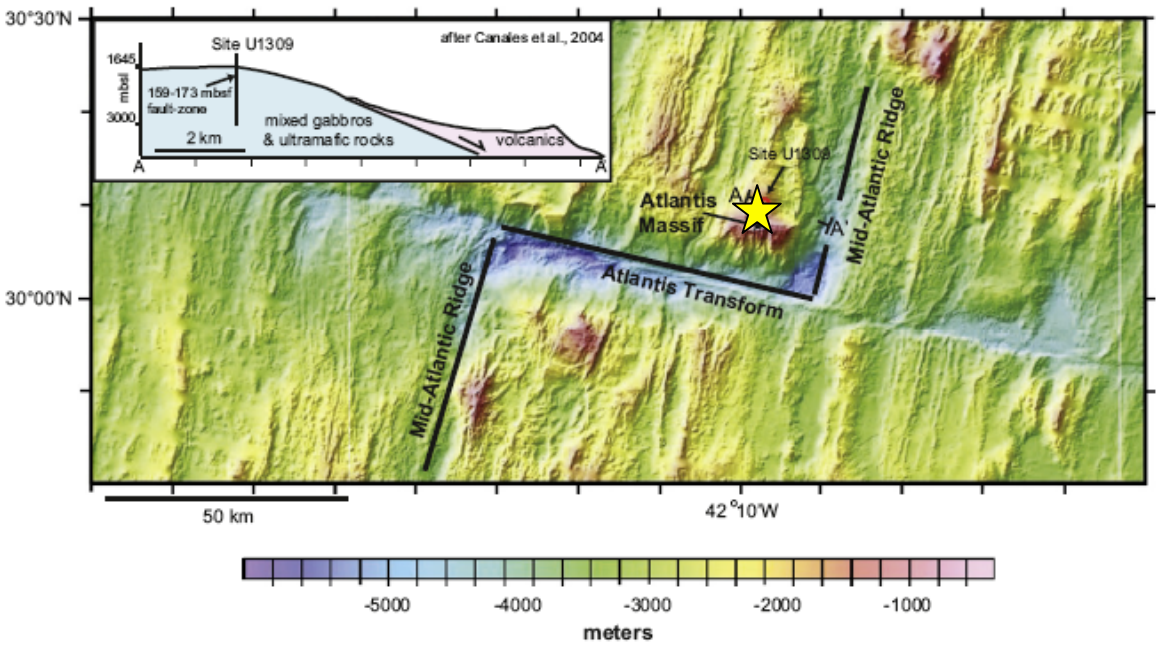

Figure 9: Bathymetric map of the Atlantis Massif located at the intersection of the Mid-Atlantic Ridge and the Atlantis Transform. Hole 1309D marked with a yellow star. Inset cross-section depicts the detachment fault of the OCC exposing the lower crustal rocks. Image modified from Hirose and Hayman (2008).

The igneous rocks are primarily younger gabbros hosted by olivine-gabbros (Figure 10) (Ildefonse et al., 2006). Gabbros within the upper 180 m are interlayered with mantle-peridotite. Troctolites, wehrlites, and dunites constitute about ~5% of the recovered rocks and are interspersed with the gabbros. Ildefonse et al. (2006) suggest that olivine-troctolites with associated poikilitic plagioclase and clinopyroxene crystals represent primitive cumulates. Diabase intrusions were emplaced late in the formation of the massif and are a major component in the upper 150 m of the core. The uppermost 380 m of core exhibit extensive alteration, in the form of amphibole veins, resulting from seawater infiltration. Evidence of alteration extends to 1415.5 mbsf, but is limited to reaction halos and single mineral replacement of olivine and pyroxene (Figure 11) (Ildefonse et al., 2006; Ildefonse et al., 2007).

Evidence for both high- and low-temperature alteration in the mineral assemblages, which reflect primarily greenschist-facies conditions, is present in the common protolith types, gabbro and serpentinized peridotite (Boschi et al., 2006). The overall alteration of the Atlantis Massif is complicated due to the combination of extensional tectonic activity and the presence of metasomatic fluids (Boschi et al., 2006). Current data available to characterize the Atlantis Massif include bulk chemical analyses of major and trace elements, conducted both onboard the research vessel and in onshore laboratories (Boschi et al., 2006; Ildefonse et al., 2006; Godard et al., 2009), and measurements of Sr and Nd isotopic concentrations (Delacour et al., 2008). An extensive array of seismic data was collected and used to interpret the structure of the massif (Ildefonse et al., 2006). To date, research efforts have focused on the composition and structure of the Atlantis Massif, but currently available

literature does not address lithium- and oxygen-isotope ratios separately or concurrently within Hole U1309D.

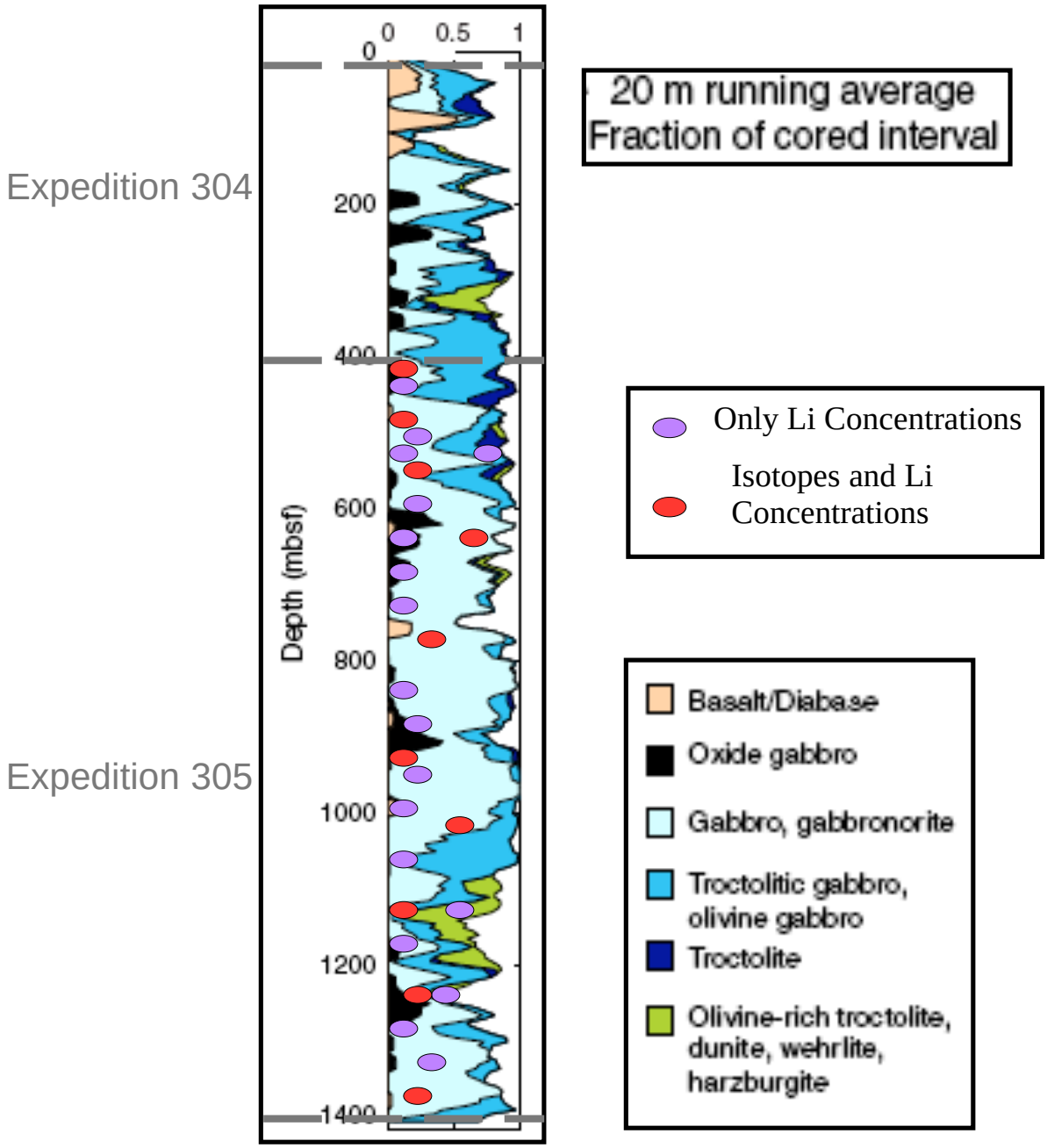

Figure 10: Stratigraphic illustration of Hole 1309D averaged every 20 m. The lithology is mainly gabbro and ultramafic rock types with intrusions of basalt. Locations of samples are marked with ovals. All samples were analyzed for lithium concentrations whereas red ovals indicate samples that were analyzed for Li and O isotopes. Image modified from Ildefonse et al. (2007).

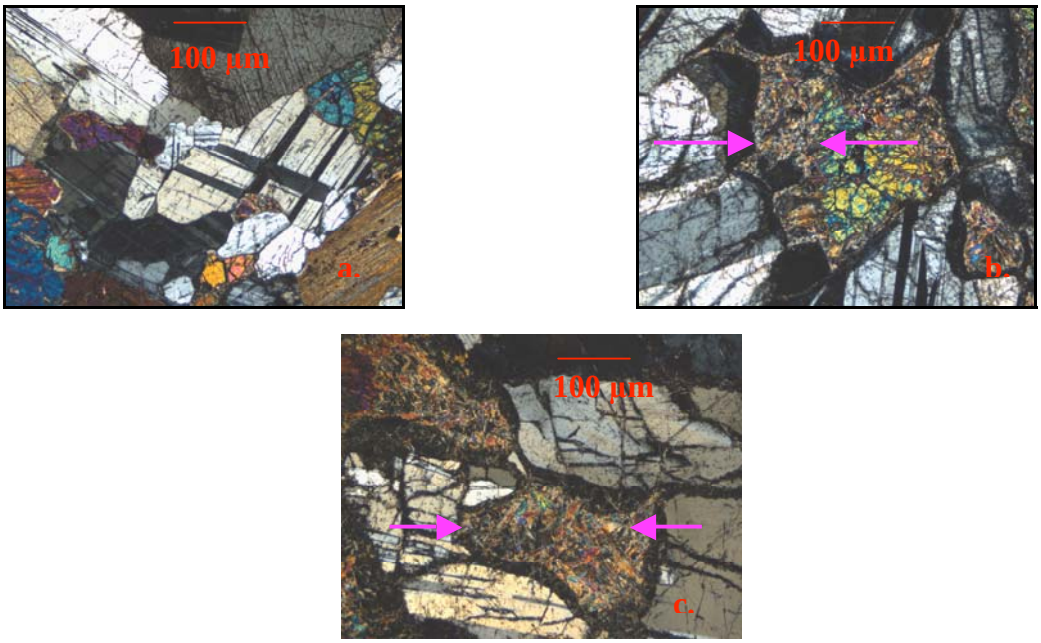

Figure 11: Photomicrographs illustrating the variation in the extent of alteration in samples from IODP Expedition 305 Hole 1309D. The extent of alteration is not systematic with depth and varies from (a) minimal (sample 22, 1137 mbsf) to (b) distinct alteration rims (sample 1, 403 mbsf), to (c) complete replacement of mineral grains by alteration phases (sample 13, 786 mbsf). Pink arrows mark the extent of alteration in a particular mineral grain.

MATERIALS AND METHODS

Core Sampling

Samples from the deeper portion of Hole 1309D (Expedition 305) were obtained from the Bremen Core Repository (BCR), Germany, which is the storage facility for Integrated Ocean Drilling Program (IODP) cores from the Atlantic region. The core is maintained in a temperature-controlled storage room and sections sampled in this study were transported to an adjoining lab for sample selection. The state and type of rock sampled was not temperature dependent, tolerating room temperatures without the risk of affecting the chemical composition of the mafic rocks. All samples were obtained from the working half of the core.

Core sections were selected at approximately 50 m increments over the 1400 m of drill core (Figure 10; Table 1). Samples within each core section were selected by their proximity to the stratigraphic position of the original shipboard geochemical analyses. The preservation of long-core continuity and ease of cutting also were considered in the selection of a sampling interval, but the selection of a specific location was kept as unbiased as possible. Each sample was cut to dimensions of approximately 4x3x2 cm and subdivided into two sections; a tabular slice was used to make a thin section and the remaining pieces formed the basis for geochemical analyses. Specific information corresponding to each sample was entered into the curator's log to document the general location, mass, and volume of sample removed. The samples were placed in labeled plastic bags and heat-sealed for transport.

Table 1: Sampling interval, depth, and rock type for samples analyzed in this study from Expedition 305 Hole 1309D. Major and trace elements, including Li concentrations, were collected for all samples. Samples chosen for isotopic analysis are in bold.

ID #	core, section, interval (cm)	depth (mbsf)	rock type
1	80, 2, 86-91	403.47	gabbro
2	87, 2, 96-104	436.62	gabbro
3	94, 3, 93-96	471.70	diabase
4	98, 3, 51-56	490.21	gabbro
5	103, 1, 22-25	511.22	diabase
6	103, 1, 27-31	511.27	gabbro
7	107, 2, 23-28	531.43	gabbro
8	117, 4, 8-12	581.84	gabbro
9	127, 1, 68-71	626.88	diabase
10	128, 3, 13-18	634.04	gabbro
11	140, 2, 33-38	689.84	wehrlite
12	150, 1, 62-66	737.22	gabbro
13	161, 2, 26-27	786.25	gabbro
14	171, 4, 36-40	836.67	gabbro
15	182, 1, 59-63	885.99	gabbro
16	193, 1, 25-30	933.65	gabbro
17	204, 4, 26-30	985.79	gabbro
18	206, 1, 5-8	991.25	diabase
19	215, 4, 24-28	1037.72	gabbro
20	225, 1, 55-61	1082.95	gabbro
21	236, 2, 109-114	1136.74	troctolite
22	236, 3, 4-6	1137.19	gabbro
23	246, 1, 78-82	1183.08	gabbro
24	256, 2, 113-117	1232.57	troctolite
25	258, 1, 106-110	1240.96	gabbro
26	267, 2, 76-80	1285.30	gabbro
27	277, 2, 114-118	1332.18	gabbro
28	287, 1, 16-19	1377.76	diabase

Sample Preparation

A billet of each sample, a slice with approximate dimensions of 4x3x1 cm, was shipped to Applied Petrographic Services, INC for thin section preparation. A portion of the subsample was ground into a coarse powder using a ceramic mortar and pestle for geochemical analysis. Powdered aliquots, (0.025 g each), of ten samples were sent to Bill McDonough at the Geochemistry Laboratory, University of Maryland, for lithium-isotope analyses. Rock chips (0.350 to 0.400 g) of the same ten samples were sent to Doug Rumble at the Geophysical Laboratory, Carnegie Institution of Washington, for oxygen-isotope analyses.

Sample Digestion

Powdered samples (0.025 g) were digested via standard nitric-hydrofluoric (HNO_3-HF) acid techniques in capped Teflon vials following the procedures outlined by Tomascak et al. (1999). Detailed procedures can be found in Appendix A and a quick reference in Appendix B. All Teflon and plastic tubes were acid washed prior to introducing the sample (Appendix C). Digested samples were dissolved into 1.0 mL 3% trace-metal-grade HNO_3. Replicate digestions were conducted for the subset of 10 samples to assess error inherent in sample preparation.

Bulk Chemical Analysis: ICP-OES

Duplicate analyses were performed on samples that were diluted to three final concentrations; 10x, 100x, and 1000x. Duplicate and replicate analyses were also conducted on the USGS Icelandic basalt (BIR-1a) rock standard (USGS Certified Standard). A Spectro Scientific ICP-OES was used to analyze the solutions with Smart Analyzer Vision Software. Global parameter settings included a modlichte nebulizer with cyclonic spray chamber, 1400 W argon plasma torch power, a pump speed of 30 rpm, and a flow rate of 1 mL/min. A 60 s, 3% trace-metal-grade HNO_3 rinse was followed by a 90 s preflush in the analyte before obtaining three consecutive measurements. Instrumental calibration concentrations were determined using either an Inorganic Ventures IV-ICPMS-71A or an Inorganic Ventures Genesis-ICAL standard solution and are summarized in Appendix D. The resulting detection limits, slopes, and intercepts for the standard regressions are presented in Appendix E, and additional information regarding the ICP-OES appears in Appendix F.

Error and Reproducibility

Results for the BIR-1a standard were compared to published values (Figure 12) to determine the precision and accuracy of each dilution. Based on this comparison, the 100x dilution appeared to best reproduce the published Li concentrations with a standard deviation of 0.65 ppm and an analytical error of 23.6%. Figure 13 illustrates the variation in Li concentrations in duplicate analyses. For lithium, a slope of 0.987 ± 0.028 indicates instrumental reproducibility at the 95% confidence level.

The variation in Li concentrations in replicate analyses is shown in Figure 14. For lithium, a slope of 0.8099 ± 0.073 indicates digestion reproducibility at the 90% confidence

interval. A notable outlier, sample 7, deviated significantly from the overall trend and skewed the remaining data. During the final steps of the digestion process a white precipitate, silicate with significant concentrations of Zr, formed when 3% HNO_3 was added. The overall lithium concentration depended on the proportion of the solid that remained insoluble, which varied between subsequent digestions.

Two samples, 21 and 24, retained small black particles at the end of the acid digestion process. SEM analysis revealed their composition to be Cr-rich spinel. A secondary electron image depicts the octahedral crystal structure as well as pitting due to acid digestion (Figure 15). It was assumed that the residuum of other samples was similar, spinel-group minerals. Li does not partition significantly into spinel, thus incomplete digestion of this phase should not influence the bulk-rock Li concentration.

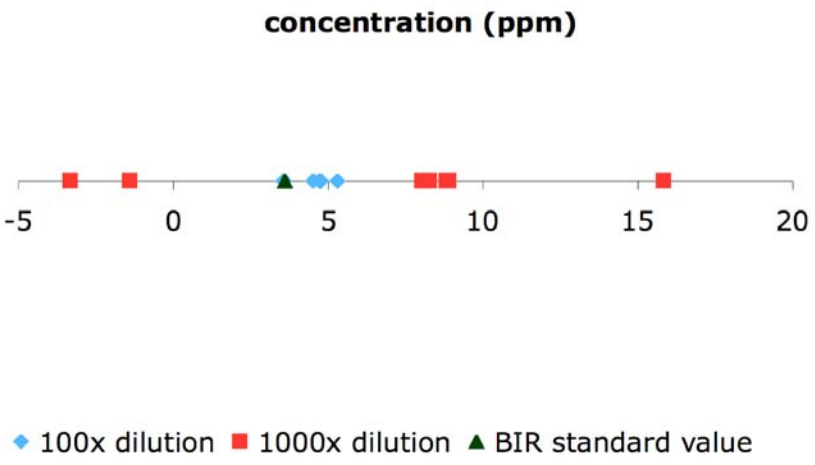

Figure 12: Plot of measured versus published lithium concentration for the rock standard BIR-1a. Green triangle denotes published concentration for the mass of standard utilized, associated error is within the symbol (3.6 ± 0.2 ppm). Red squares represent 1000x diluted, digested standard and blue diamonds represent 100x diluted, digested standard. Each symbol denotes a separate run of the same sample on the ICP. The 100x dilution is more precise and closer to the published value for lithium in the BIR-1a standard than the 1000x dilution. For comparative purposes, lithium values obtained from the 100x dilution were used. This same process was applied to all analyzed elements.

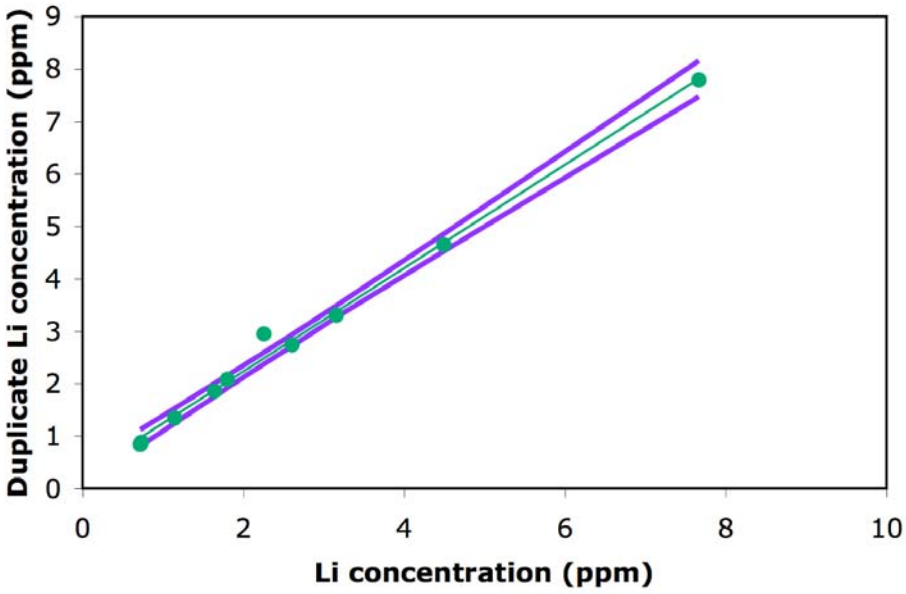

Figure 13: Duplicate versus original lithium concentration data (ppm) for a subset of 10 samples. Duplicates represent samples from a single digestion but different dilutions. A linear-least-squares fit of the data resulted in a slope of 0.987 ± 0.028. This indicates that the ICP-OES is able to reproduce lithium concentration data.

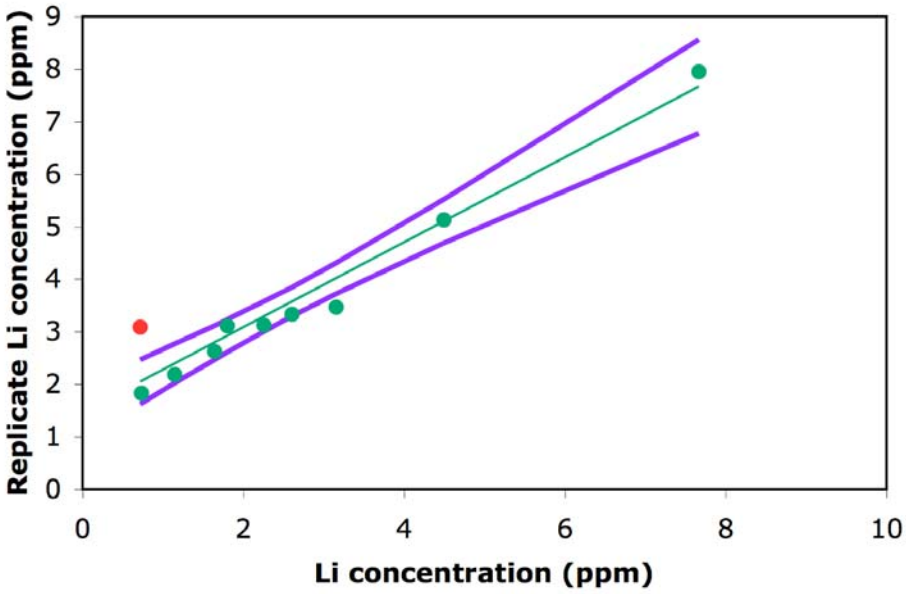

Figure 14: Replicate versus original lithium concentration data (ppm) for a subset of ten samples. The linear-least-squares fit of the data was 0.8099 ± 0.073. The relative reproducibility of lithium data between digestions is good. However, sample 7, noted in red, deviates significantly from the general trend. During digestion sample 7 would inconsistently precipitate a white solid once 3% HNO_3 was added in the last step.

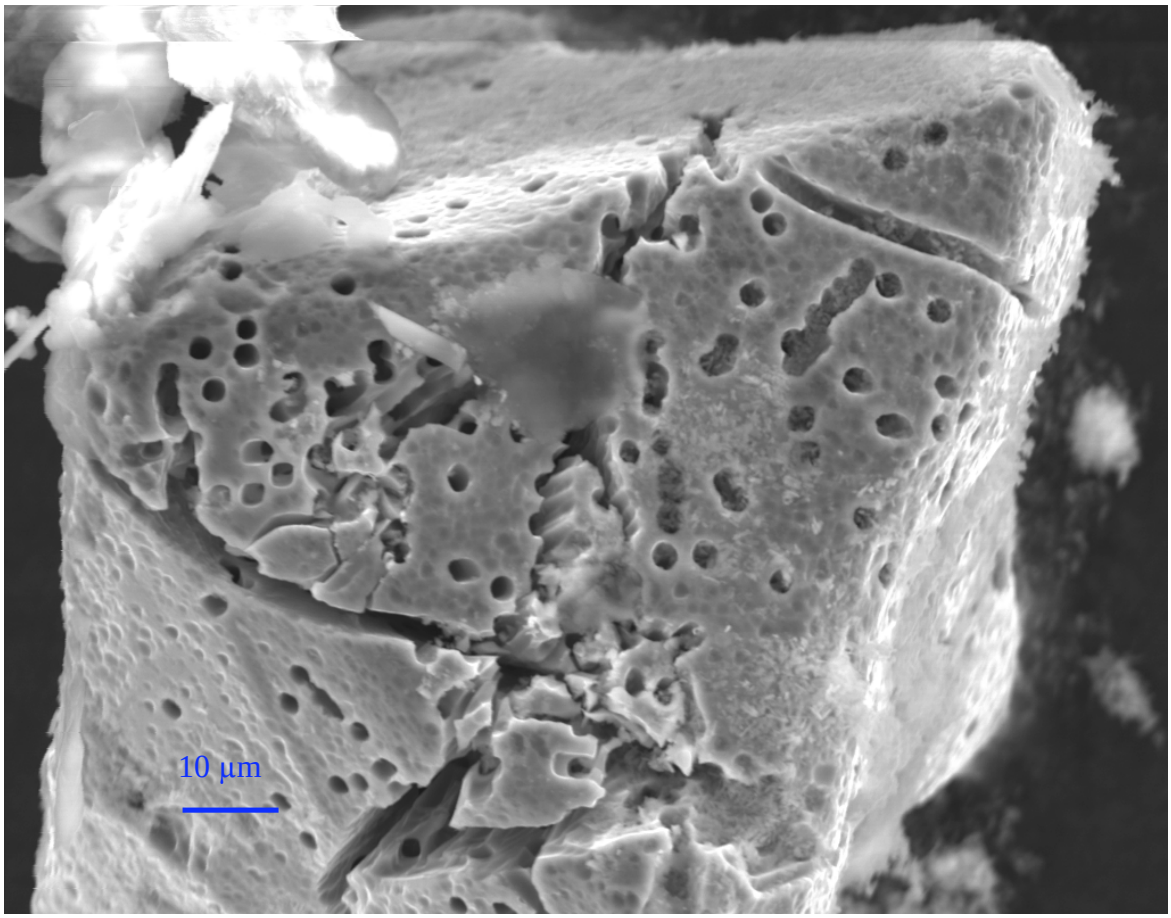

Figure 15: Secondary electron image obtained on the SEM of the Cr-spinel from the residuum of sample 21. Note the octahedral crystal structure and pitting due to partial digestion.

RESULTS AND DISCUSSION

Lithium Concentrations and Li and O Isotopes in Hole 1309D

Lithium concentrations for samples analyzed from Hole 1309D range from 0.72 to 16.71 ppm with an average of 3.82 ppm and a standard deviation of 3.07 ppm (Table 2). Lithium concentrations exhibit no significant systematic trend when examined with depth in the drill core (Figure 16). Furthermore, the concentrations cluster near the unaltered MORB lithium concentration value of 3.5 ppm (Tomascak et al., 2004). An outlier with significantly higher lithium concentration, sample 11 (16.71 ppm), occurs at 689.84 mbsf within a documented fault zone.

Figure 17 illustrates the $\delta^{18}O$ and $\delta^{7}Li$ values for the subset of ten samples with depth in the drill core. The two solid lines represent the unaltered MORB values for $\delta^{18}O$ and $\delta^{7}Li$ (5.5 ‰ and 4 ‰, respectively) (Eiler, 2001; Tomascak et al., 2004). The dashed horizontal lines denote fault zones between 108 and 126 mbsf, 685 and 785 mbsf, and at 1100 mbsf in the drill core (Blackman et al., 2006). The values for $\delta^{18}O$ and $\delta^{7}Li$ are significantly and consistently less than unaltered MORB for most of the core. Exceptions include samples 7 and 25, at 531 and 1241 mbsf, respectively, which record isotopically heavier $\delta^{7}Li$ values. Although $\delta^{18}O$ and $\delta^{7}Li$ trends are similar (i.e., are coupled) throughout a majority of the drill core, the two isotopic systems are decoupled on a local scale.

Lithium concentrations and isotopes are directly compared in Figure 18. No apparent correlation exists between the datasets with depth in the drill core.

Table 2: Results for Li concentrations of all samples and O- and Li-isotopic ratios of ten selected samples analyzed in this study.

ID #	$d^{18}O$ (‰ SMOW)	$d^{7}Li$ (‰ LSVEC)	Li (ppm)
1	3.695	-0.5	7.66
2			2.86
3	3.235	-0.2	1.64
4			4.01
5			3.36
6			1.47
7	2.14	7.1	0.72
8			2.35
9			4.35
10	0.985	-1.5	1.15
11			16.71
12			5.56
13	1.905	-2.7	3.16
14			3.60
15			3.21
16	4.31	-0.7	4.49
17			3.79
18			5.39
19	5.045	2.6	2.60
20			4.70
21			2.51
22	3.78	2.6	2.26
23			4.68
24			2.77
25	3.47	6.1	0.73
26			7.12
27			2.26
28	2.08	-0.6	1.80

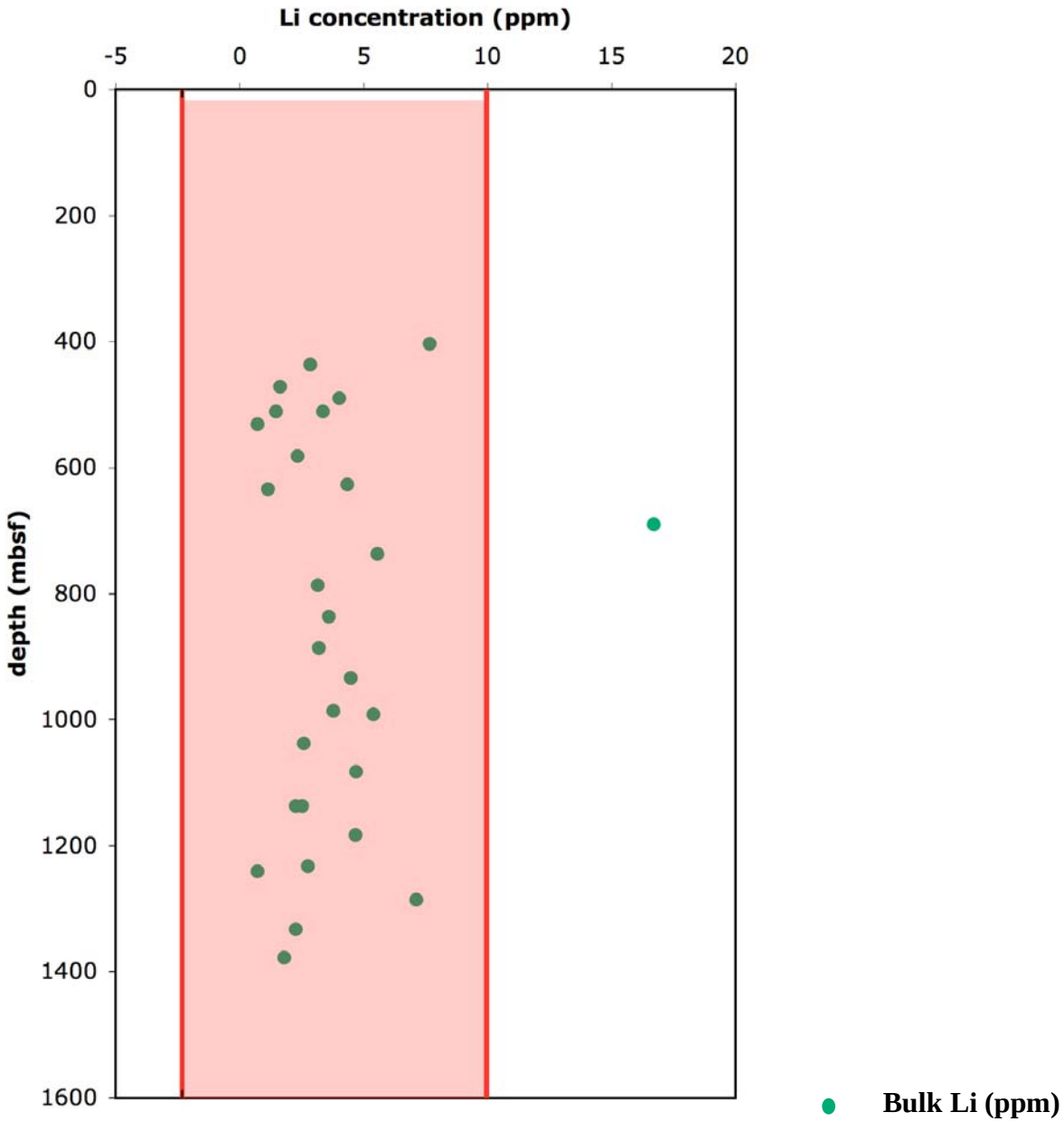

Figure 16: Plot of lithium concentration data for all Hole 1309D samples. The 2σ range is noted in red. No significant monotonic trend is apparent with depth, and, except for sample 11, values do not deviate significantly from the unaltered MORB value of ~ 3.5 ppm.

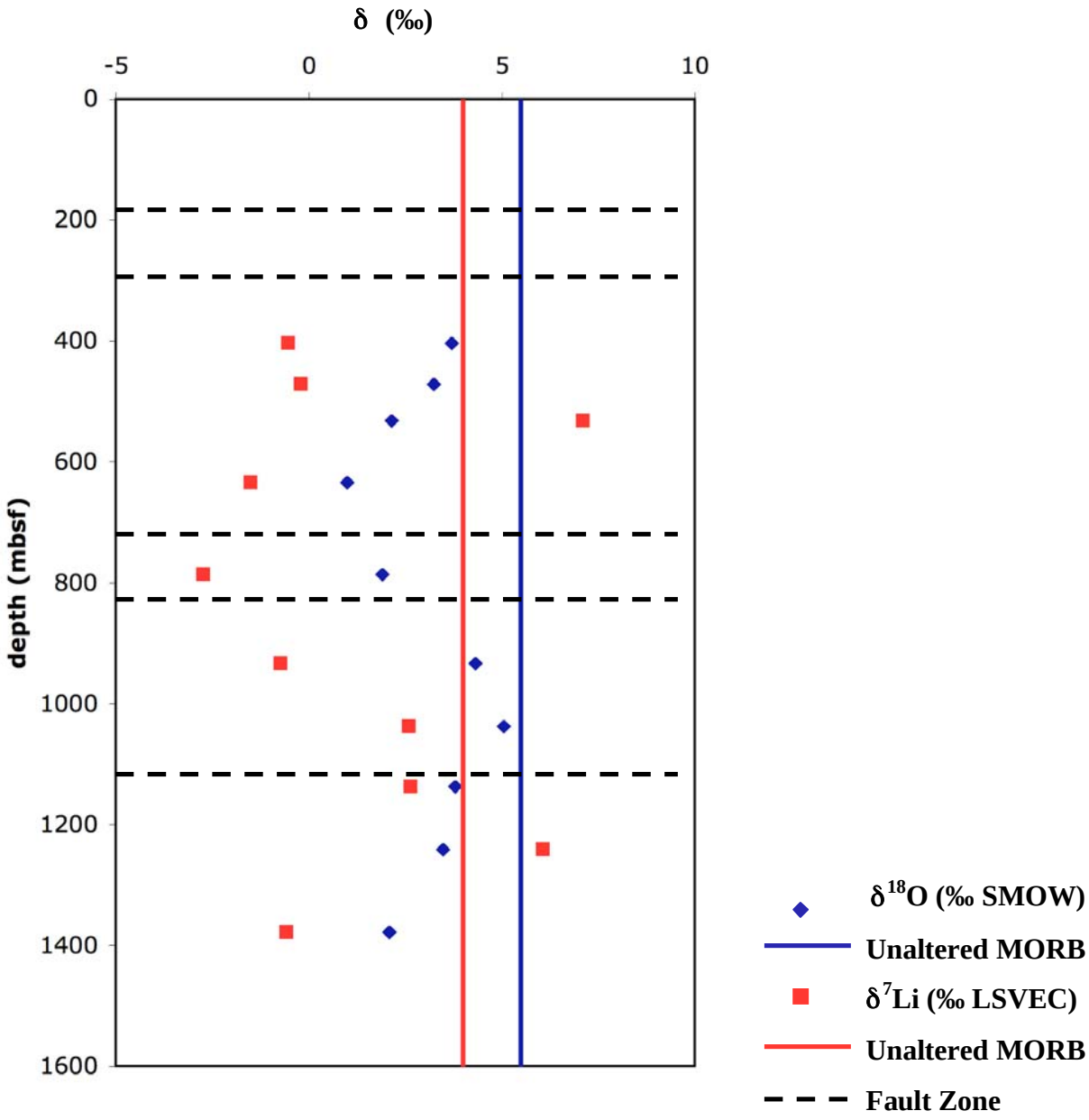

Figure 17: Lithium-and-oxygen isotope ratios with depth (mbsf) in Hole 1309D. Solid lines represent the respective unaltered MORB values for lithium and oxygen. Dashed lines represent fault zones within the drill core. Generally, lithium and oxygen isotopic compositions vary systematically with depth and are significantly and consistently lighter than the unaltered MORB signature, indicating that high-temperature hydrothermal alteration affected this portion of the lower crust. Localized decoupling of O and Li is indicated by the two samples whose Li isotopes are heavier than unaltered MORB without a concordant increase in O isotopes.

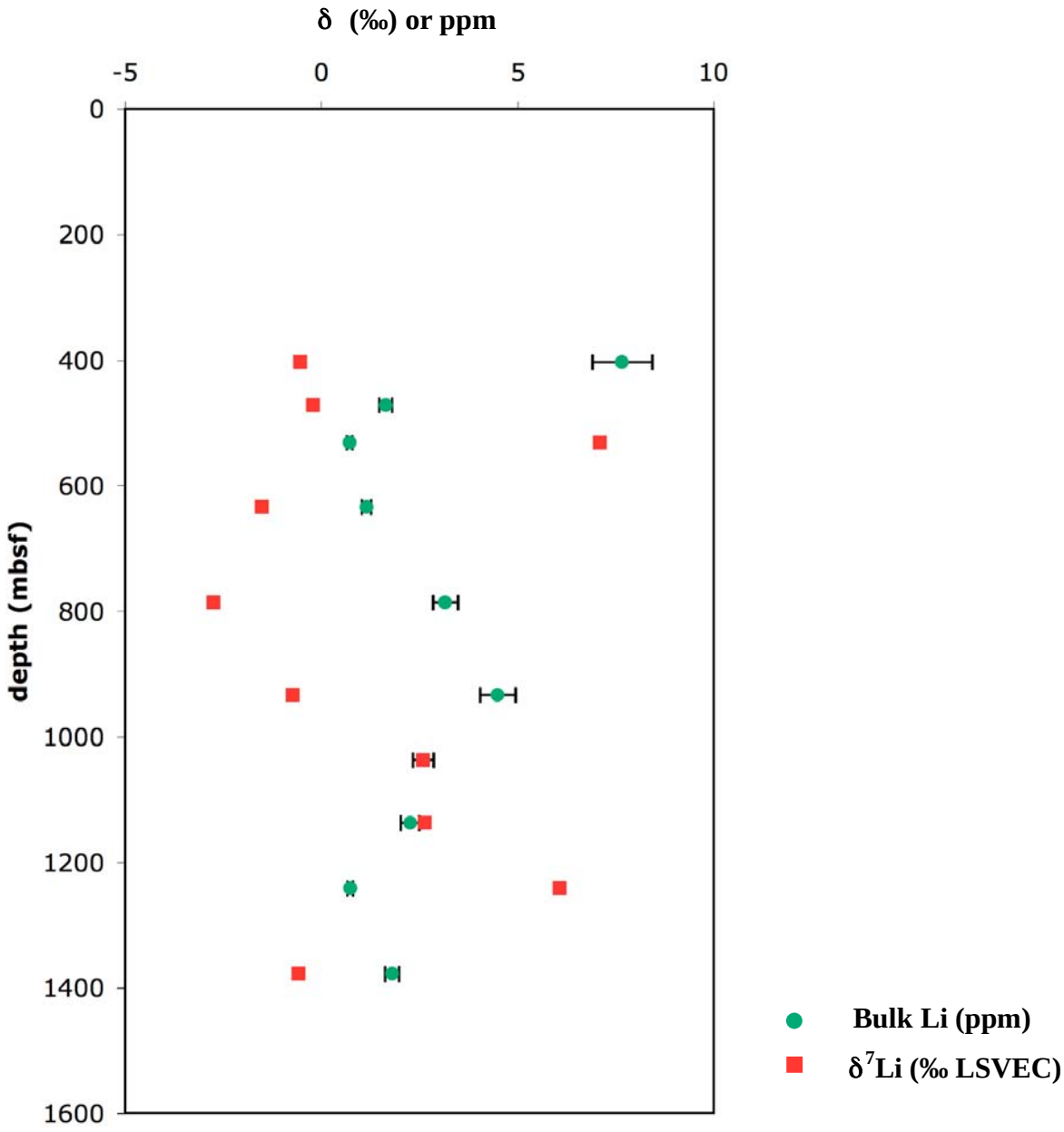

Figure 18: Lithium concentrations (ppm) and lithium isotope ratios (per mil) with depth in Hole 1309D. Bulk lithium concentration data plotted with 10% error and the error for lithium-isotope is within the data points. Lithium concentration values fall within the reported range for unaltered MORB (~ 3.5 ppm). There is no apparent correlation between Li concentrations and isotopic ratios, indicating that bulk lithium concentration is not dependent on the degree of hydrothermal alteration.

Interpretations and Comparative Analysis

Systematic trends with depth for $\delta^{18}O$ and $\delta^{7}Li$ and values consistently lighter than unaltered MORB indicate the occurrence of high-temperature alteration throughout the portion of the drill core sampled. Although isotopically heavy values, observed in $\delta^{7}Li$, are typically indicative of low-temperature hydrothermal alteration, no fractures that might facilitate low-temperature fluids at these depths were documented. Replicate $\delta^{18}O$ analyses of the same samples had small standard deviations, implying that the process responsible for elevated $\delta^{7}Li$ did not cause a concurrent elevation in $\delta^{18}O$ values. Without a means to facilitate low-temperature alteration, and the lack of evidence supporting sample heterogeneity, the most likely explanation for the localized decoupling is chemical evolution of the fluid. The lack of correlation between Li concentrations and isotopes implies that bulk Li concentration is dependent on factors other than the degree of hydrothermal alteration.

Holes 504B, 1256D, 894G-F, and 735B were chosen for comparative analysis with the results from Hole 1309D for the following reasons. Holes 504B and 1256D are from fast-spreading centers associated with the EPR that do not penetrate Layer 3 gabbros. However, Li and O isotopes are well characterized in Hole 504B and demonstrate coupling of the isotopic systems within the upper oceanic crust. Hole 1256D penetrates to the Layer 2-to-3 transition and has well documented Li concentration data. Hole 894G-F is also from a fast-spreading center near the EPR but samples Layer 3 gabbros characterized by O isotopes. Oxygen isotopic data is also available for Hole 735B that samples an OCC at a slow-spreading center along the SW Indian Ridge.

Fast-spreading centers

Expeditions 69/70/83/111/140/148 Hole 504B

Figure 4 represents a comparison of $\delta^{18}O$ and $\delta^{7}Li$ signature profiles within Hole 504B along a fast-spreading segment of the Costa Rica Rift. This drill core samples Layers 1 and 2 of the oceanic crust. The $\delta^{18}O$ and $\delta^{7}Li$ trends are coupled with depth within the upper crust. The response of both element systems to changes in the temperature of alteration is evident in the change of the isotope ratios from heavy to light with the transition from low- to high-temperature alteration. Lithium concentration data (Figure 5) positively correlates with $\delta^{7}Li$ values, wherein Li concentration increases as Li is incorporated into alteration phases, heavy isotope preferred. This occurs during low-temperature alteration. Under high-temperature conditions Li is leached, heavy isotope preferred (Chan et al., 2002). This indicates that Li concentration is responsive to temperature-dependent hydrothermal alteration reactions within the upper crust. Both Li concentration and $\delta^{7}Li$ values return to unaltered MORB values in the lower dike portion of the drill core.

$\delta^{7}Li$ values range from 3.4 to 4.7 ‰ and -1.7 to 2.4 ‰ in the volcanic and dike sections of 504B, respectively (Chan et al., 2002). For Hole 1309D, $\delta^{7}Li$ values range from -2.7 to 2.6 ‰. This range includes much lighter isotopic ratios than Hole 504B indicating higher temperatures of alteration or greater volumes of fluid interacting with the rock. The lighter isotopic range is not surprising because Hole 1309D extends to the lower oceanic crust while Hole 504B is restricted to the upper crust. Not only are they different lithologically, but the initial geothermal gradient would have caused greater temperatures at depth in the lower crust. During high-temperature alteration lithium is expected to leach

from the rock favoring the heavy isotope resulting in a positive correlation between lithium concentration and δ^7Li values. However, a lack in correlation between lithium concentration and δ^7Li within Hole 1309D (Figure 18) implies that the concentrations and isotopes of lithium respond differently to the conditions of alteration at depth in the crust. The two reported heavy δ^7Li outliers, 6.1 and 7.1 ‰, are significantly heavier than the highest values in the range for the volcanic section of Hole 504B. This indicates the influence of high fluid flux or evolving fluid composition on the resulting isotopic signature (Gao et al., 2006).

Expedition 147 Hole 894F-G

Hole 894F-G sampled the lower oceanic crust at a structurally complex intra-plate ridge at the junction between the Pacific, Nazca, and Cocos plates (Gillis et al., 2001). The δ^{18}O profile for Hole 894F-G does not vary in any systematic way with depth (Figure 6). The δ^{18}O values of gabbros are lighter than unaltered MORB, 2.2 to 5.0 ‰, with one exception, 6.5 ‰, that is located in close proximity to a vein network. The remaining δ^{18}O values that are similar to or heavier than unaltered MORB are associated with olivine basalts (Lecuyer and Reynard, 1996). Generally, oxygen and strontium isotope values remain coupled during low-temperature alteration. However, decoupling of this relationship during high-temperature alteration was most likely due to diffusional processes and the limited availability of water at depth in the crust (Lecuyer and Reynard, 1996). Similar processes could be responsible for decoupling Li and O isotopic systems during dehydration reactions at subduction zones (Tomascak et al., 2004; Marschall et al., 2007).

The range in δ^{18}O values in Hole 894 gabbros is similar to that of Hole 1309D gabbros, 0.985 to 5.045 ‰. The δ^{18}O range for Hole 1309D incorporates lighter

compositions that could be due to structural or petrological differences between the two drill sites. The heterogeneity in the range of $\delta^{18}O$ values also could have resulted from differences in spreading rate between Hole 894 and Hole 1309D and the expression of the lower crust at the seafloor. The chemistry of the fluid at depth could have been significantly different from seawater, affecting the composition changes due to fluid-rock reactions.

Agrinier et al. (1995) dismiss the depleted ^{18}O compositions of serpentinized peridotites present at Hole 894 because they assumed that the occurrence of peridotites is not characteristic of the oceanic crust. However, the exploration of OCCs indicates that peridotites and serpentinized lower-crustal rocks are present on the seafloor and interact with seawater. Although Agrinier et al. (1995) suggest that only Layer 2 is involved in elemental and isotopic exchange with the seawater, the distinct trends represented in the lower-crustal rocks of Hole 1309D indicate that the lower crust is interacting with seawater. This affected its chemical composition and needs to be considered in any mass-balance calculation.

Lecuyer and Reynard (1996) suggest that temperature is a major constraint for the probability and extent of isotopic exchange between a fluid and rock body. This indicates that variation in isotopic values could be sub-classified within the high- and low-temperature alteration designations based on minor temperature and fluid-flux variations.

Expeditions 309/312 Hole 1256D

Hole 1256D sampled the EPR, penetrating to a depth of 1500 mbsf, and will be extended in 2011 to drill through the dike-gabbro transition to become the first drill core to sample Layers 1, 2, and 3 of the oceanic crust. Gao et al. (2009) presented Li concentration data, but Li and O isotopic data are not available for Hole 1256D (Figure 7). The lithium

concentration values are generally lower than the average for unaltered MORB, 3.5 ppm. The values tend to decrease with depth, indicative of high-temperature alteration leaching Li from the rock. At a depth of approximately 1400 mbsf, Li concentrations increase rapidly to values similar to and greater than unaltered MORB (Gao et al., 2009). A fault zone near 1100 mbsf could have acted as a conduit for increased fluid flow or interactions with fluids with evolving compositions, resulting in a greater extent of alteration.

Lithium concentration values for Hole 1309D (Figure 16) cluster near the unaltered MORB value of 3.5 ppm, however, there are more samples with concentrations lower than 3.5 than above 3.5. Thus, the Li concentration data could be reflecting the overall occurrence of high-temperature alteration, similar to that observed in the lower portions of Hole 1256D. The anomalously high Li concentration, 16.71 ppm at 689 mbsf, is similar to the deviation noted in Hole 1256D and could result from a similar structural or petrological control.

Slow-spreading centers

Expedition 118/176 Hole 735B

Hole 735B sampled an OCC along the SW Indian Ridge. $\delta^{18}O$ compositions for mineral separates of plagioclase, clinopyroxene, and olivine were determined for the length of the drill core and compared with their corresponding unaltered MORB values (Figure 8) (Gao et al., 2006). Plagioclase, being the most responsive to hydrothermal alteration, was used for general comparison purposes. Below 800 mbsf $\delta^{18}O$ exhibits minimal deviation from the unaltered MORB value. A slight deviation to 4 ‰ occurs at a depth of 723 mbsf

and can be associated with a series of faults. Gao et al. (2006) conclude that this deviation resulted from the rock body reacting with high temperature fluids (i.e., seawater).

Similarly, the greatest deviation from unaltered MORB in Hole 1309D (0.985 ‰) could be associated with a fault zone. However, several other fault zones exist in both Hole 735B and Hole 1309D that do not demonstrate similarly depleted ^{18}O values. This discrepancy could be a function of sampling or it could indicate that other factors influence O isotopic ratios, such as fluid volume and chemistry or closure of a fault.

Summary

Isotopic signatures of a rock body record the ability of fluid to interact with the rock via chemical reactions. Structural controls, such as faults and fractures, can have a significant effect on the ability of a fluid to circulate within a rock body. Other points of weakness, such as mineral grain boundaries, can act as a conduit for minimal fluid flow or foci for geochemical reactions. Whether reactions are rock- or fluid-dominated, having either a low or high water-to-rock ratio, respectively, will also affect how alteration is expressed within a sample. In fluid-dominated reactions there is sufficient recharge of circulating fluid to minimize the effects of changing chemistry. The opposite is true for rock-dominated regimes that experience large changes in fluid chemistry as the reaction progresses. However, high fluid fluxes can cause immobile elements to become mobile after equilibrium is reached for the mobile elements (Delacour et al., 2008). Layer 3 gabbros tend to undergo rock-dominated chemical reactions resulting in alteration halos on olivine and pyroxene (Figure 11). Variation in chemistry of the alteration phases could demonstrate multiple iterations of alteration with evolving fluid chemistry over time (Morishita et al.,

2009). The capability of a rock body to maintain the rock-dominated alteration signature depends on whether subsequent lower-temperature alteration is facilitated (Lecuyer and Reynard, 1996).

With the exception of two anomalously heavy δ^7Li values, Li and O isotope ratios are coupled with depth in the lower oceanic crust sampled at Hole 1309D. No systematic trend in Li concentration data is observed with depth, and deviations from unaltered MORB could result from variations in fluid flux and/or chemistry. The same explanations, along with analysis of heterogeneous samples, can be applied to the δ^7Li deviations.

The δ^7Li values for Hole 1309D are lower than those reported in 504B, verifying that hydrothermal alteration in the lower crust occurred at a higher temperature than that in the upper crust (Chan et al., 2002; Tomascak et al., 2004). Minimal variation in Li concentration data for 1309D from the unaltered MORB value, of 3.5 ppm, indicates that different factors, such as fluid volume and chemistry, control the partitioning of Li in the rocks. The Li concentration results for Hole 1309D are similar to the values obtained from the deepest portions of Hole 1256D. The δ^{18}O ranges for Hole 894 and Hole 1309D are similar with the exception of a few lighter δ^{18}O values for Hole 1309D. These differences could be due to spreading rate or fluid chemistry in each of the gabbroic sections. Hole 735B exhibits δ^{18}O values and trends with depth completely different than Hole 1309D even though their structural setting is similar. Although the spreading rate differs between the Atlantis Massif and the drill cores referenced for comparative analysis, it is not clear whether this trait, specifically, is the cause for the observed variations.

CONCLUSION

IODP Expedition 305 Hole 1309D samples an OCC that exposes a continuous lower-crustal sequence on the seafloor along the MAR. A subset of ten samples spanning the length of core yield $\delta^{18}O$ and $\delta^{7}Li$ ranges of 0.985 to 5.045 ‰ and -2.7 to 2.6 ‰, respectively. With the exception of two anomalously heavy $\delta^{7}Li$ values (531 and 1241 mbsf), the $\delta^{7}Li$ and $\delta^{18}O$ systems are coupled with depth and are significantly lighter than their respective unaltered MORB values. Li concentrations for these samples range from 1.32 to 12.37 ppm and exhibit no systematic correlation with $\delta^{7}Li$ with depth. The $\delta^{18}O$ values from Hole 1309D are similar to those from Hole 896, EPR, but different than Hole 735B, SW Indian Ridge. Li concentration values within Hole 1309D do not positively correlate with $\delta^{7}Li$ values as found in Hole 504B (Chan et al., 2002) or exhibit a distinct trend with depth as in 1256D (Gao et al., 2009).

Li and O isotopes follow similar trends in the lower- crust samples at the Atlantis Massif. The values are lighter than unaltered MORB, indicating the occurrence of high-temperature alteration (Tomascak et al., 2004). The observation that Li and O isotopic ratios are coupled in both the upper and lower crust at mid-ocean ridges implies that processes and reactions occurring in subduction zones are responsible for the decoupling observed in convergent margin lavas (Chan et al., 2002; Ryan and Kyle, 2004; Williams et al., 2009). The localized decoupling observed in samples 7 and 25 from Hole 1309D are attributed to fluid composition departing from that of seawater. Evolution of fluid composition is most probable at greater depths where conduits for fluid are limited. Hydrothermal reactions in this environment would be rock-dominated and result in chemical evolution of the fluid

interacting with the rock. Although localized decoupling is observed, whether it is volumetrically significant for determining the isotopic signature of the average lower oceanic crust depends on corroborating studies in other ocean basins.

The lightest isotopic values are spatially correlated with a fault zone at depth. These faults, along with fractures and other zones of weakness in the crust, facilitate fluid movement to lower portions of the crust allowing fluid-dominated hydrothermal reactions to occur. However, not all of the fault zones exhibit similarly significant deviations, implying that they are sealed and no longer good fluid conduits.

Although differences exist among crustal segments from spreading centers of variable rates, the heterogeneity within a single segment indicates that factors such as fluid temperature, chemistry, and fluid-rock ratios are most likely responsible for the observed variations. Li and O bulk-rock isotopes, alone, are not able to quantify these parameters. Future work analyzing mineral separates and other isotopic systems, such as strontium, could illuminate the effects of fluid volume and temperature. Additional work focusing on the chemistry of fluid inclusions in alteration phases could reveal the chemical composition of the alteration fluids and provide insight to the fluid composition and better constrain the extent of alteration.

LITERATURE CITED

Agrinier, P., Hékinian, R., Bideau, D., and Javoy, M., 1995. O and H stable isotope compositions of oceanic crust and upper mantle rocks exposed in the Hess Deep near the Galapagos Triple Junction. Earth and Planetary Science Letters. 136, 183-196.

Alt, J.C., Muehlenbachs, K., and Honnorex, J., 1986. An oxygen isotope profile through the upper kilometer of the oceanic crust, DSDP 504B. Earth and Planetary Science Letters. 80, 217-229.

Bach, W., and Humphris, S.E., 1999. Relationship between Sr and O isotope compositions of hydrothermal fluids and the spreading and magma-supply rates at oceanic spreading centers. GEOLOGY. 27, 1067-10-70.

Blackman, D.K., Ildefonse, B., John, B.E., Ohara, Y., Miller, D.J., McLeod, C.J., and the Expedition 304/305 Scientists. Site U1309. Proceedings of the Integrated Ocean Drilling Program. 304/305, 1-509.

Boschi, C., Früh-Green, G.L., Delacour, A., Karson, J.A., and Kelley, D.S., 2006. Mass transfer and fluid flow during detachment faulting and development of an oceanic core complex, Atlantis Massif (MAR 30°N). Geochemistry Geophysics Geosystems. 7, 1-39.

Boschi, C., Dini, A., Früh-Green, G.L., Kelley, D.S., 2008. Isotopic and element exchanges during serpentinization and metasomatism at the Atlantis Massif (MAR 30°N): Insights from B and Sr isotope data. Geochimica et Cosmochimica Acta. 72, 1801-1823.

Chan, L., Alt, J.C., and Teagle, D.A.H., 2002. Lithium and lithium isotope profiles through the upper oceanic crust: a study of seawater-basalt exchange at ODP Sites 504B and 896A. Earth and Planetary Science Letters. 201, 187-201.

Chan, L., and Frey, F.A., 2003. Lithium isotope geochemistry of the Hawaiian plume; results from the Hawaii Scientific Drilling Project and Koolau Volcano. Geochemistry Geophysics Geosystems. 4. 20 p.

Delacour, A., Früh-Green, G.L., Frank, M., Gutjajr, M., Kelley, D.S., 2008. Sr- and Nd-isotope geochemistry of the Atlantis Massif (30°N, MAR): Implications for fluid fluxes and lithospheric heterogeneity. Chemical Geology. 254, 19-35.

Eiler, J.M., 2001. Oxygen isotope variations of basaltic lavas and upper mantle rocks. In: Valley, J.W., Cole, D.R. (Eds.), Stable Isotope Geochemistry. Mineralogical Society of America and Geochemical Society, Washington DC, United States. 43, 319-364.

Elliott, T., Jeffcoate, A., Bouman, C., 2004. The terrestrial Li isotope cycle: light-weight constraints on mantle convection. Earth and Planetary Science Letters. 220, 231-245.

Escartín, J., Cowie, P.A., Searle, R.C., Allerton, C., Mitchell, N.C., MacLeod, C.J., and Slootweg, A.P., 1999. Quantifying tectonic strain and magmatic accretion at a slow spreading ridge segment, Mid-Atlantic Ridge, 29°N. Journal of Geophysical Research. 104, 10421-10437.

Flesch, G.D., Anderson, A.R., and Svec, H.J., 1973. A secondary isotopic standard for $^{6}Li/^{7}Li$ determinations. International Journal or Mass Spectrometry and Ion Physics. 12, 265-272.

Gao, Y., Hoefs, J., Przybill, R., and Snow, J.E., 2006. A complete oxygen isotope profile through the lower oceanic crust, ODP Hole 735B. Chemical Geology. 233, 217-234.
Gao, Y., Huang, J., and Casey, J.F., 2009. Data report: trace element geochemistry of oceanic crust formed at superfast-spreading ridge, Hole 1256D. Proceedings of the Integrated Ocean Drilling Program. 309/312, 1-10.
Gillis, K.M., 1995. Controls on hydrothermal alteration in a section of fast-spreading oceanic crust. Earth and Planetary Science Letters. 134, 473-489.
Gillis, K.M., Muchlenbachs, K., Stewart, M., Gleeson, T., and Karson, J., 2001. Fluid flow patterns in fast spreading East Pacific Rise crust exposed at Hess Deep. Journal of Geophysical Research. 106, 26311-26329.
Godard, M., Awaji, S., Hansen, H., Hellebrand, E., Brunelli, D., Johnson, K., Yamasaki, T., Maeda, J., Abratis, M., Christie, D., Kato, Y., Mariet, C., and Rosner, M., 2009. Geochemistry of a long in-situ section of intrusive slow-spread oceanic lithosphere: Results from IODP Site U1309 (Atlantis Massif, 30°N Mid-Atlantic Ridge). Earth and Planetary Science Letters. 1-13.
Hirose, T., and Hayman, N.W., 2008. Structure, permeability, and strength of a fault zone in the footwall of an oceanic core complex, the Central Dome of the Atlantis Massif, Mid-Atlantic Ridge, 30°N. Journal of Structural Geology. 30, 1060-1071.
Ildefonse, B., Blackman D., John, B.E., Ohara, Y., Miller, D.J., MacLeod, C.J., and the IODP Expeditions 304-305 Scientists, 2006. IODP Expeditions 304 and 305 Characterize the lithology, structure, and alteration of an oceanic core complex. Scientific Drilling. 3, 4-11.
Ildefonse, B., Blackman D., John, B.E., Ohara, Y., Miller, D.J., MacLeod, C.J., and the IODP Expeditions 304-305 Scientists, 2007. Oceanic core complexes and crustal accretion at slow-spreading ridges. GEOLOGY. 35, 623-626.
Kobayashi, K., Tanaka, R., Morigutii, T., Shimizu, K., and Nakamura, E., 2004. Lithium, boron, and lead isotope systematics of glass inclusions in olivines from Hawaiian lavas: evidence for recycled components in the Hawaiian plume. 212, 143-161.
Lecuyer, C., and Reynard, B., 1996. High-temperature alteration of oceanic gabbros by seawater (Hess Deep, ocean Drilling Program Leg 147): Evidence from oxygen isotopes and elemental fluxes. Journal of Geophysical Research. 101, 15883-15897.
Marschall, H.R., Pogge von Strandmann, P.A.E., Seitz, H.M., Elliot, T., and Niu, Y., 2007. The lithium isotopic composition of orogenic eclogites and deep subducted slabs. Earth and Planetary Science Letters. 262, 563-580.
Morishita, T., Hara, K., Nakamura, K., Sawaguchi, T., Tamura, A., Arai, S., Okino, K., Takai, K., and Kumagai, H., 2009. Igneous, alteration and exhumation processes recorded in abyssal peridotites and related fault rocks from an oceanic core complex along the Central Indian Ridge. Journal of Petrology. 50, 1299-1325.
Neo, N., Yamazaki, S., and Miyashita, S., 2009. Data report: bulk rock compositions of samples from the IODP Expedition 309/312 sample pool, ODP Hole 1256D. Proceedings from the Integrated Ocean Drilling Progam. 309/312, 1-24.
Ryan, J.G., and Kyle, P.R., 2004. Lithium abundance and lithium isotope variations in mantle sources: insights from intraplate volcanic rocks from Ross Island and Marie Byrd Land (Antarctica) and other oceanic islands. Chemical Geology. 212, 125-142.
Shanks, W.C., 2001. Stable isotopes in seafloor hydrothermal systems: vent fluids, hydrothermal deposits, hydrothermal alteration, and microbial processes. In: Valley,

J.W., Cole, D.R. (Eds.), Stable Isotope Geochemistry. Mineralogical Society of America and Geochemical Society, Washington DC, United States. 43, 470-525.
Tang, Y., Zhang, H., and Ying, J., 2007. Review of the lithium isotope system as a geochemical tracer. International Geology Review. 49, 374-388.
Tomascak, P.B., Carlson, R.W., and Shirey, S.B., 1999. Accurate and precise determination of Li isotopic compositions by muli-collector sector ICPMS. Chemical Geology. 158, 145-154.
Tomascak, P.B., Ryan, J.G., and Defant, M.J., 2000. Lithium isotope evidence for light element decoupling in the panama subarc mantle. GEOLOGY. 28, 507-510.
Tomascak, P.B., et al., 2002. Lithium isotope sample preparation. University of Maryland, Department of Geology protocol. 1-6.
Tomascak, P.B., 2004. Developments in the understanding and application of lithium isotopes in the Earth and planetary sciences. In: Johnson, C.M., Beard, B.L., and Albarède, F. (Eds.), Geochemistry of Non-Traditional Stable Isotopes. Mineralogical Society of America and Geochemical Society, Washington DC, United States. 55, 153-195.
Tremblay, A., Meshi, A., and Bedard, J.H., 2009. Oceanic core complexes and ancient oceanic lithosphere: Insights from Iapetan and Tethyan ophiolites (Canada and Albania). Tectonophysics. 473, 36-52.
Wilcock, W.S.D., and Delaney, J.R., 1996. Mid-ocean ridge sulfide deposits: Evidence for heat extraction from magma chambers or cracking fronts? Earth and Planetary Science Letters. 145, 49-64.
Williams, H.M., Nielsen, S.G., Renac, C., Griffin, W.L., O'Reilly, S.Y., McCammon, C.A., Pearson, N., Viljoen, F., Alt, J.C., and Halliday, A.N., 2009. Fractionation of oxygen and iron isotopes by partial melting processes: Implications for the interpretation of stable isotope signatures in mafic rocks. Earth and Planetary Science Letters. 283, 156-166.
Wilson, D.S., Teagle, D.A., Alt, J.C., Banerjee, N.R., Umino, S., Miyashita, S., Acton, G.D., Anma, R., Barr, S.R., Belghoul, A., Carlut, J., Christie, D.M., Coggon, R.M., Cooper, K.M., Cordier, C., Cripini, D.M., Durand, S.R., Einaudi, F., Galli, L., Gao, Y., Geldmacher, J., Gilber, L.A., Hayman, N.W., Herrero-Bervera, E., Hirano, M., Holter, S., Ingle, S., Jiang, S., Kalberkamp, U., Kerneklian, M., Koepke, J., Laverne, C., Lledo Vasquez, H.L., Maclennan, J., Morgan, S., Neo, N., Nichols, H.J., Park, S.H., Reichow, M.K., Sakuyama, T., Sano, T., Sandwell, R., Schibner, B., Smith-Duque, C.E., Swift, S.A., Tartarotti, P., Tikku, A.A., Tominaga, M., Veloso, E.A., Yamasaki, T., Yamazaki, S., and Ziegler C., 2006. Drilling to gabbro in intact ocean crust. SCIENCE. 312, 1016-1020.
Winter, J.D., 2001. An Introduction to Igneous and Metamorphic Petrology.Upper Saddle River, NJ, Prentice Hall, 697p.

APPENDICES

Appendix A: Standard HNO_3-HF Acid Digestion

Day 1: 0.025 g of sample was weighed and transferred to a 15 mL Teflon vial. Both the cap and vial were labeled with the sample identification number. 15 drops of trace-metal-grade concentrated nitric acid (HNO_3) was added making sure to wash the sample from the side of the vial. Using a Teflon dropper bottle, 2 mL (66 drops) of trace-metal-grade hydrofluoric acid (HF) was added. The vial was capped and placed on a hotplate overnight at 100°C. The temperatures listed throughout are those of the digital readout, which was approximately 15 degrees higher than the actual surface temperature of the hotplate. The surface of the hotplate exhibited a temperature gradient of 10 degrees between the edge and the center.

Day 2: The Teflon vials were gently swirled and tapped to collect sample and fluid in the bottom of the vial. The vials where held up to the light and carefully rotated to verify that only a white solid (SiF_4) remained. Any samples with dark solids were placed in the sonicator until only white solid remained. The caps were removed carefully using tongs to grip the vial and minimize risk of HF dripping from the cap. The samples were dried down (4 to 6 hours) at 110°C forming a cake of white solid at the bottom of the vial. 15 drops of concentrated HNO_3 were added swirling the vials to break up the sample cake. The sample dissolved and was dried down (1.5 hours) at 110°C. 1.5 mL (45 drops) of trace-metal-grade concentrated hydrochloric acid (HCl) was added to each vial swirling to break up the sample cake and break down the SiF_4. At this point the samples are a transparent yellow liquid with a dissolving white solid. The vials were capped and returned to the hotplate and allowed to reflux at 100°C overnight or for a weekend swirling periodically. A 1:3 mixture of HNO_3 and HCl (18 and 48 drops respectively) can be used if dissolving the white solid is problematic.

Day 3: The samples were swirled and held up to the light to check for remaining white solid. The sample was dried down halfway (1.5 to 2 hours) at 110°C. 10 drops of concentrated HCl was added and the sample was checked again for white solid. If no solid was present the

sample was completely dried down. Sample was dried to the point where the yellow solid was glossy or resinous, being careful not to burn the edges. If white solid remained the sample was dried down half way and 10 more drops of concentrated HCl was added. Consecutive drying down and HCl additions were repeated until the white solid completely dissolved. The samples were placed in a sonicator, so that only the bottom of the vials is covered with water, to expedite the process by breaking up remaining white solid. 6 drops of 3% trace-metal-grade HNO_3 was added to the dried down sample. The vial was swirled and lightly heated until the cake dissolved. 4 more drops of 3% HNO_3 were added and the vial capped and checked for any white solid. If solid was present the sample was dried down and the consecutive HCl treatment repeated. If no solid was present the sample was transferred to a labeled 15 mL Falcon tube. The Teflon vial was rinsed with 15 and then 8 drops of 3% HNO_3 to ensure complete transfer of sample. The total dilution volume was increased to 10 mL by the addition of 9mL of 3% HNO_3. Additional dilutions of 100x and 1000x (l mL into 10 mL total then repeated) were created to ensure that major Earth elements did not exceed the calibration curve established on the ICP-OES.

Appendix B: Reynolds Lab Acid Digestion Protocol

1. Weigh out powdered sample (~25 mg) into labeled Teflon vial

2. Add **15** drops concentrated trace-metal-grade **HNO_3** and **66** drops concentrated **HF**. Cap and set on hotplate at ~100°C (thermostat) overnight (longer periods necessary for some samples).

3. Uncap and dry down.

4. Break up solid with **15** drops **HNO_3**. Swirl and sonicate as necessary.

5. Dry down.

6. Add **18** drops **HNO_3** and **48** drops concentrated trace-metal-grade **HCl**. Cap and place on hotplate at ~100°C (thermostat) overnight.

7. Swirl vials, hold on side up to the light, and rotate to check for solids. Be careful not to get any samples in the cap or ribbing.

If no solids are present proceed to step 8a.

If white solids are present proceed to step 8b.

8a. Dry down half way and add **10** drops **HCl**. Check for solids.

If no solids are present proceed to step 9a. (Small dark solids are acceptable)

If there are white solids present proceed to step 8b.

8b. Sonicate and check for solids.

If no solids are present go to step 8a.

If solids are present add more **HCl**, sonicate and/or reflux, then go to step 7.

9. Dry down until glossy.

10. Add **6** drops trace-metal-grade **3% HNO_3**, swirl, heat slightly then add **4** more drops **3% HNO_3**.

11. Hold up to the light and check for solids.

If no solids are present proceed to step 12a.

If solids are present let sit overnight. Check for solids.

When solids are absent proceed to step 12a.

When solids are present proceed to step 12b.

12a. Transfer to acid washed 15mL falcon tube.

12b. Sonicate and/or dry down then add **10** drops **HNO_3**, swirl and go to step 9.

(Alternative: **5** drops **HNO_3** and **15** drops **HCl** then go back to step 8a.)

13. Rinse the Teflon vial with **15** drops **3% HNO_3** rolling the vial carefully to capture the entire sample. Transfer to corresponding falcon tube.

14. Rinse the Teflon vial with **8** drops **3% HNO_3**. Transfer to corresponding falcon tube.

15. Cap the falcon tube and place in test-tube rack.

16. Dilute and extract needed volumes for dilutions.

Helpful Hints:

Swirling the vials assists breaking up the solid faster.

Sonicating agitates the samples but also heats them causing minimal refluxing.

Minimal heating warms the solution enough to help the solid dissolve.

A combination of the above is best to accelerate the dissolving process.

Know whether to expect organic compounds, if suspected, first bake samples.

Pay attention to the temperature on the dial versus thermostat.

Teflon melts at 210°C while the falcon tube caps melt at just over 130°C.

Appendix C:

Teflon Cleaning Protocol

1. Remove labels being careful not to scratch the Teflon. Ethyl alcohol can be used to remove the marker.
2. Rinse the vials 3 times with 18.0 ohm (Milli-Q) water making sure to rinse the caps and the ribbing.
3. Add enough 6M reagent grade HCl to cover the bottom of the vial, approximately 1.5mL, cap and let reflux for at least 90 minutes, preferably overnight, at 100°C.
4. Pour acid back into wash acid storage.
5. Rinse vials and caps 3 times with Milli-Q water.
6. Add enough 7M reagent grade HNO_3 to cover the bottom of the vial, approximately 1.5mL, cap and let reflux for at least 90 minutes, preferably overnight, at 100°C.
7. Pour acid back into wash acid storage.
8. Rinse vials and caps 3 times with Milli-Q water

Cleaning Protocol for Other Plastics

1. Pour enough 7M reagent grade (or 3% trace-metal-grade) HNO_3 in each container to cover the bottom and partially fill the container. For 15 mL falcon tubes approximately 1-2 mL is needed.
2. Reflux at 95°C (thermostat temperature) for at least 2 hours.
3. Rinse container and cap with Milli-Q water.
4. Pour small amount of 5% trace-metal-grade HNO_3 into each container, cap, and agitate. For 15 mL falcon tubes use approximately 1-1.5 mL is necessary.
5. Rinse container and cap with Milli-Q water.
6. Dry completely before transferring samples or reagents.

Appendix D: ICP-OES Calibration Elements

Elements used to calibrate the ICP-OES and the three concentrations from which the calibration curve was constructed. The standard solutions were obtained from Inorganic Ventures.

			Element Concentration					
	element	symbol	0 ppb	20 ppb	50 ppb	100 ppb	250 ppb	500 ppb
IV-ICPMS-71A	aluminium	Al	X			X		X
	boron	B	X			X		X
	barium	Ba	X			X		X
	beryllium	Be	X			X		X
	cobalt	Co	X			X		X
	chromium	Cr	X			X		X
	cesium	Cs	X			X		X
	copper	Cu	X			X		X
	iron	Fe	X			X		X
	gallium	Ga	X			X		X
	potassium	K	X			X		X
	manganese	Mn	X			X		X
	nickel	Ni	X			X		X
	lead	Pb	X			X		X
	strontium	Sr	X			X		X
	vanadium	V	X			X		X
	zinc	Zn	X			X		X
	calcium	Ca	X			X		X
	magnesium	Mg	X			X		X
	sodium	Na	X			X		X
	dysprosium	Dy	X			X		X
	europium	Eu	X			X		X
	gadolinium	Gd	X			X		X
	lanthinum	La	X			X		X
	samarium	Sm	X			X		X
	ytterbium	Yb	X			X		X
Genesis-ICAL	titanium	Ti	X			X		X
	silicon	Si	X			X		X
	yttrium	Y	X			X		X
	molybdenum	Mo	X		X		X	
	lithium	Li	X	X		X		

Appendix E: ICP-OES Standard Regressions and Detection Limits

Standard curve data for selected elements run on the ICP-OES. BEC is the background equivalence coefficient, DL is the detection limit in ppb for the element, and A0 and A1 represent the slope and intercept of the regression.

Line (nm):	BEC: ppb	DL: ppb	Corr.Coef.:	Range: ppb	MDL ppb	CRQL ppb	A0:	A1:
Al 167.078	4.06	0.0737	0.99999	0.0737 - 600	5.00000	5.00000	-0.59667	0.0018622
B 249.773	17.9	0.165	1	0.165 - 600	25.00000	25.00000	-1.2764	0.0016143
Ba 455.404	3.8	0.0356	0.99996	0.0356 - 600	5.00000	5.00000	-0.50381	0.00013087
Be 313.042	4.82	0.0368	1	0.0368 - 600	5.00000	5.00000	-3.8778	4.16E-05
Co 228.616	17.7	0.213	1	0.213 - 600	5.00000	5.00000	0.34017	0.0012933
Cr 267.716	21.5	0.248	1	0.248 - 600	5.00000	5.00000	-0.29068	0.0031049
Cs 455.531	3.8	0.0356	0.99996	0.0356 - 600	5.00000	5.00000	-0.12198	0.00013127
Cu 324.754	31.9	0.316	1	0.316 - 600	5.00000	5.00000	-14.369	0.00080065
Fe 259.941	13.9	0.123	0.99999	0.123 - 600	5.00000	5.00000	-0.82791	0.0013476
Ga 141.444	70.5	0.2	0.99995	0.2 - 600	15.00000	15.00000	44.63	0.42122
K 766.491	89.1	1.56	1	1.56 - 600	5.00000	5.00000	3.8508	0.0039356
Mn 257.611	3.02	0.0112	1	0.0112 - 600	5.00000	5.00000	-0.27488	0.00033116
Ni 231.604	29	0.438	0.99999	0.438 – 600	5.00000	5.00000	0.30645	0.0022271
Pb 220.353	92.8	1.39	1	1.39 – 600	5.00000	5.00000	-2.1207	0.011114
Sr 407.771	1.39	0.0287	0.99998	0.0287 – 600	5.00000	5.00000	-0.20889	1.80E-05
V 292.464	37.2	0.145	1	0.145 – 600	5.00000	5.00000	-2.5428	0.0030653
Zn 213.856	8.85	0.135	1	0.135 – 600	5.00000	5.00000	-0.54396	0.0012909
Ca 315.887	83.7	0.692	1	500 - 5e+003	10.00000	10.00000	- 0.017366	0.002994
Ca 396.847	7.27	0.264	0.99999	0.264 – 600	10.00000	10.00000	-6.6349	1.94E-05
Mg 279.553	1.31	0.014	1	0.014 - 2.6e+003	5.00000	5.00000	-0.85414	4.58E-05
Na 589.592	78.5	1.39	0.9999	1.39 – 600	45.00000	45.00000	-34.626	0.00052772
Dy 353.170	35.6	0.646	0.99998	0.646 – 600	5.00000	5.00000	0.34582	0.00040102
Eu 420.505	22.5	0.375	0.99999	0.375 – 600	5.00000	5.00000	0	0.00021843

Appendix E Continued

Line (nm):	BEC: ppb	DL: ppb	Corr.Coef.:	Range: ppb	MDL ppb	CRQL ppb	A0:	A1:
Gd 342.247	63.4	1.18	1	1.18 – 600	5.00000	5.00000	-1.0902	0.0010343
La 408.672	55.6	0.721	0.99999	0.721 – 600	5.00000	5.00000	-0.38167	0.00071469
Nd 401.225	181	3.23	0.99999	3.23 - 600	5.00000	5.00000	0.55757	0.0027476
Sm 359.260	112	2.11	0.99999	2.11 - 600	15.00000	15.00000	-111.93	0.0022553
Yb 328.937	2.73	0.0401	1	0.0401 - 600	5.00000	5.00000	-2.8017	9.55E-05
Li 670.780	3.79	0.0694	0.99986	0.0694 - 120	5.00000	5.00000	-3.6776	8.46E-05
Ti 334.941	6.86	0.0927	1	0.0927 - 600	5.00000	5.00000	-6.769	0.00036845
Si 288.158	254	4.4	0.99987	4.4 - 600	10.00000	10.00000	-253.45	0.0098668
Al 176.641	151	1.47	0.99999	1.47 - 600	5.00000	5.00000	-0.59653	0.075627
Y 371.030	6.39	0.0999	0.99999	0.0999 - 600	5.00000	5.00000	-6.2632	0.00011898
Y 377.433	13.9	0.298	0.99997	0.298 - 600	5.00000	5.00000	-13.627	0.00017635
Y 360.073	10.3	0.191	0.99998	0.191 - 600	5.00000	5.00000	-10.108	0.0001942
Mo 202.095	17.5	0.232	0.99997	0.232 - 300	5.00000	5.00000	-17.347	0.002935
Mo 203.909	29.9	0.368	0.99994	0.368 - 300	5.00000	5.00000	-29.763	0.0047524

Appendix F: Additional ICP-OES Information

Elements in IV-ICPMS -71A element standard: (all 10 ppm) Ag, Al, As, B, Ba, Be, Ca, Cd, Ce, Co, Cr, Cs, Cu, Dy, Er, Eu, Fe, Ga, Gd, Ho, K, La, Lu, Mg, Mn, Na, Nd, Ni, P, Pb, Pr, Rb, S, Se, Sm, Sr, Th, Tl, Tm, U, V, Yb, Zn

Elements in Genesis I-CAL standard: (50 ppm) S; (10 ppm) Ce, Cu, Eu, Fe, In, K, Ni, P, Si, Ti, V, Y, Zr; (5 ppm) Mn, Mo, Na, Sc; (2 ppm) Be, Li, Sr

Data retrieval:

In Analysis view, highlight data and select export. Check boxes on right side of window, making sure that ASCII (.ade) files will be created and open in corresponding folder on desktop (Reynolds ICP data). Open excel and select the data tab. Designate that text files will be imported from the folder where data was saved and open the data file.

Calibration data retrieval:

In the methods-calibration menu select file-print. Indicate the information you would like to print (standarization-overview) and check the .rtf extension box. The file can then be opened in Microsoft Word.